IMPLEMENTING A PIEZOELECTRIC TRANSFORMER FOR A FERROELECTRIC PHASE SHIFTER CIRCUIT

ANTHONY M. ROBERTS

Bachelor of Electrical Engineering

Cleveland State University

May, 2008

Submitted in partial fulfillment of requirements for the degree

MASTER OF SCIENCE IN ELECTRICAL ENGINEERING

at the

CLEVELAND STATE UNIVERSITY

December, 2011

This thesis has been approved
for the Department of Electrical and Computer Engineering
and the College of Graduate Studies by

_____

Thesis Committee Chairperson, Dr. Fuquin Xiong

_____

Department/Date

_____

Dr. Robert Romanofsky

_____

Department/Date

_____

Dr. Ana Stankovic

_____

Department/Date

_____

Dr. Nigamanth Sridhar

_____

Department/Date

DEDICATION

To the glory of the Lord Jesus Christ, through who's love I have been so blessed.

ACKNOWLEDGEMENTS

For all this work and everything wonderful it has brought into my life, I owe Dr. Bob Romanofsky a debt of gratitude I can never repay. As a mentor he has given me invaluable guidance on research, my career, and life. His own work and accomplishments are an inspiration and motivate me to continue learning and always seek out new opportunities. I am grateful for his friendship, because as long as I "love NASA and the space program and humanity" he'll always be in my corner.

There is no greater comfort that the love of my parents and that they have been, and will be, there for me. My achievements are their achievements.

Many thanks to the staff of NASA Glenn whose technical help and company I have come to appreciate so much. Many thanks to Liz Mcquaid, Fred Van Keuls, Max Scardeletti, Nick Varaljay, and George Ponchak.

I owe much to the faculty and staff at Cleveland State University's Department of Electrical and Computer Engineering for the time, patience, help, and lab resources that allowed me to accomplish this work.

A special thanks to Alicia Pavlecky for reviewing my grammar and style.

A very special thanks to Bill Witt and Joe Rymut. Whether it was badgering me to finish my work, your guaranteed willingness to go out for beer, or providing a relieving distraction, you were there. Good friends like these are far and few between.

Thanks be to God, through whom all things are possible.

IMPLEMENTING A PIEZOELECTRIC TRANSFORMER FOR A FERROELECTRIC PHASE SHIFTER CIRCUIT

ANTHONY ROBERTS

ABSTRACT

The ferroelectric phase shifter is the fundamental component in a new type of scanning phased array, the ferroelectric reflectarray. These phase shifters require a DC bias voltage, up to 300 Vdc, for continuous 0 to 360 degree phase shift. In a conventional phased array comprised of potentially thousands of phase shifters, each phase shifter requires up to six control signals so routing and integration become extremely complex. The coplanar ferroelectric phase shifters require only a single control signal, albeit at high voltage. If a technology could be developed that allows a low-level signal to be routed to each phase shifter and converted to the proper bias voltage levels, essentially at the phase shifter, then a new type of phased array architecture could be realized.

Magnetic circuit components comprise a conventional means for voltage and current step-up and step-down. However, magnetic devices suffer from resistive (I^2R) losses, and dimensional and economical costs, thereby forcing compromises in design

and cost. Integrated multichannel, high voltage amplifiers have been developed for the MEMs industry and are usually based on high voltage Op Amp arrays. The goal of this work, however, is to demonstrate low power, high voltage control to complement the inherent high efficiency of the ferroelectric reflectarray.

This research explores using a piezoelectric transformer (PT) as the alternative enabling component in the voltage supply for a ferroelectric phase shifter utilizing piezoelectrics in an AC-DC converter. Unlike magnetic transformers PTs generate no electromagnetic interference, have higher efficiencies, and have higher power densities.

Preliminary work consisted of characterizing the device under cryogenic conditions due to the temperature-dependant dielectric constant of ferroelectrics and ultimately realistic environmental conditions. Then an analysis of the equivalent PT model is performed focusing on reconciling the theoretical results with the experimental and extracting the equivalent circuit parameters for the point of operation. Next, in a proof-of-concept application, a circuit was developed for using the PT in a driver for a ferroelectric phase shifter.

Initial results were successful with the driver achieving an output voltage from 0 to over 400 Vdc while accomplishing 0 to 115 degrees phase shift at Ka-band frequencies (phase shift was limited to less than a full 2π because of phase shifter design).

Future work includes, further characterizing the piezoelectric transformer, improving the driver circuit, implementing an output voltage feedback control scheme, and using the driver in a ferroelectric phased array antenna.

TABLE OF CONTENTS

Page

ABSTRACT……...V

NOMENCLATURE..... XII

LIST OF TABLES IX

LIST OF FIGURES X

I INTRODUCTION 1

1.1 Background 1

1.2 Problem Formulation 21

1.3 Thesis Organization 22

II CHARACTERIZING THE MLPT 24

2.1 Motivation..... 24

2.2 Experimental Characterization: Procedure and Results..... 27

III PT MODELING AND SIMULATION 43

3.1 Overview..... 43

3.2 Static Operation 45

3.3 Dynamic Operation..... 52

IV DRIVER CIRCUIT DESIGN..... 56

4.1 Theory of Operation and Design..... 56

4.2 Prototype Performance Evaluation 60

4.3 Integration with the Ferroelectric Phase Shifter 63

V CONCLUSION..... 67

5.1 Summary..... 67

5.2 Future Research and Work..... 69

REFERENCES..... 73

APPENDIX..... 75

LIST OF TABLES

Table **Page**

Table 1: Characteristics for the SMMTF53P2S40 Piezoelectric Material..... 18

Table 2: PT Equivalent Component Values..... 49

Table 3: PT Equivalent Component Experimental Values 50

Table 4: PT Equivalent Component Curve-Fitting Results 51

LIST OF FIGURES

Figure **Page**

Figure 1: X-band Ferroelectric Reflectarray 2

Figure 2: Thin Film Ferroelectric Phase Shifter 3

Figure 3: Crystal Lattice Cell of $BaTiO_3$ 5

Figure 4: Deformation of Cell Followed by Polarization 5

Figure 5: The 616 Element Reflectarray Controller Connected to the Reflectarray 7

Figure 6: Element Controller with High Voltage Switching IC 8

Figure 7: Lead Zirconate Titanate Elementary Cell 9

Figure 8: Piezoelectric Poling in Weiss Domains 10

Figure 9: Designation of the Axes and Directions of Deformation 11

Figure 10: A Rosen-type Piezoelectric Transformer 15

Figure 11: Equivalent Circuit Model for the Piezoelectric Transformer 17

Figure 12: Mechanical Drawings for the SMMTF53P2S40 Multilayer PT 19

Figure 13: Cryostat and Instrumentation 28

Figure 14: PT Setup for Cryogenic Testing 29

Figure 15: PT Frequency Response at 298 K 30

Figure 16: PT Cryogenic Frequency Response 31

Figure 17: PT Cryogenic Split Resonance Frequency Response 33

Figure 18: PT Input Impedance Magnitude 35

Figure 19: PT Input Impedance Phase Angle 36

Figure 20: LR200 Coherent Laser Radar. 38

Figure 21: Dimension Measurement Results 38

Figure 22: Experimental and Simulated (Mnfr.) Frequency Responses 46

Figure 23: Experimental and Simulated (Mnfr.) Frequency Responses (Tuned) 47

Figure 24: Experimental and Simulated (Exp.) Frequency Responses 48
Figure 25: Experimental and Simulated (Exp.) Frequency Responses (Tuned) 48
Figure 26: Curve fitting Frequency Response 50
Figure 27: PT Gain as a Function of n 53
Figure 28: Input Impedance Magnitude as a Function of n 54
Figure 29: Complete schematic for proof-of-concept driver circuit 58
Figure 30: Complete Phase Shifter Driver Circuit 60
Figure 31: Driver Circuit Voltage Output For Fixed Fin and Variable Vin 61
Figure 32: Driver Circuit Voltage Output for Fixed Vin and Variable Fin 62
Figure 33: Fin = 42.79 kHz, 0.1 Vdc Applied, 139.21 Degrees Phase Shift Result 64
Figure 34: Fin = 46.01 kHz, 1.0 Vdc Applied, 139.39 Degrees Phase Shift Result 64
Figure 35: Fin = 50.48 kHz, 10.0 Vdc Applied, 144.98 Degrees Phase Shift Result 65
Figure 36: Fin = 52.21 kHz, 50.0 Vdc Applied, 165.71 Degrees Phase Shift Result 65
Figure 37: Fin = 52.82 kHz, 100.0 Vdc Applied, -179.24 Degrees Phase Shift Result 66
Figure 38: Fin = 53.46 kHz, 300.0 Vdc Applied, -123.10 Degrees Phase Shift Result 66
Figure 39: Coupled Mass-Spring-Damper System 75
Figure 40: PT Dual-Resonance Time Domain Response 77
Figure 41: PT Dual-Resonance Frequency Domain Response 77
Figure 42: Equivalent Electrical Circuit 78

NOMENCLATURE

DC: Direct current

AC: Alternating current

Vdc: Direct current volts

Vac: Alternating current volts

V/V: Volts per Volt

PT: Piezoelectric transformer

IC: Integrated circuit

RTD: Resistance temperature detector

MLPT: Multilayer piezoelectric transformer

GBP: Gain bandwidth product

CHAPTER I

INTRODUCTION

1.1 Background

A phased array is a type of antenna made electronically steerable by means of constructive and destructive interference from electromagnetic waves emitted by multiple elements on the antenna. Its surface is composed of many phase shifters that become active with a certain phase delay. It is this delay between the phase shifters that facilitates the interference pattern necessary to steer the beam. The range of frequencies for which the antenna operates determines the details of its construction. The advantages of the phased array over a gimbaled parabolic antenna are the elimination of moving parts, rapid beam steering, better integration, and packaging flexibility [1].

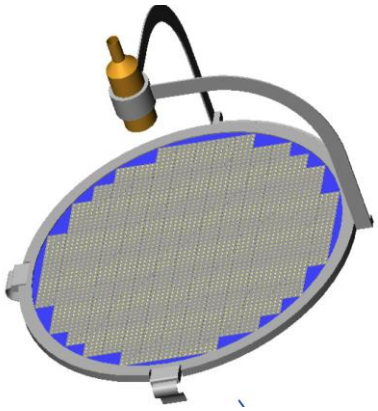

Figure 1: X-band Ferroelectric Reflectarray

The reflectarray is an improvement being pioneered at NASA's Glenn Research Center by Dr. Robert Romanofsky. It is a phased array antenna (Figure 1) but with the directly radiating array replaced by a feed horn that illuminates a reflective surface in transmission and collects the reflections off the surface in the receiving mode [2]. The novelty of this application is in the elements that make up the reflectarray surface and accomplish the beam steering. In a conventional phased array, the phase shifters are located between the amplifiers and radiating elements. A modulated signal from a single source is distributed to the phase shifters through some type of manifold. This type of array is called direct radiating. The phase shifter loss is unimportant because the phase shifters follow the low noise amplifiers in the case of a receiving array and precede the power amplifiers in the case of a transmitting array. Consequently they do not play a part in determining the sensitivity or noise temperature in the former, nor do they significantly affect efficiency in the latter. In a reflectarray, the phase shifters are located between the amplifier and the radiators, therefore they determine sensitivity and efficiency, and their insertion loss is of paramount importance. Conventional commercial monolithic microwave integrated circuit phase shifters have an insertion loss approaching or

exceeding 10 dB at Ka-band, rendering a reflectarray with such devices impractical. NASA Glenn has developed low loss phase shifters based on thin ferroelectric films, an example of which is shown in Figure 2. This device is the motivation behind this research.

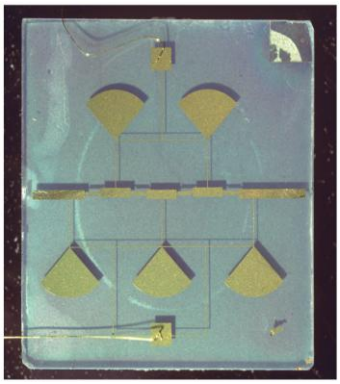

Figure 2: Thin Film Ferroelectric Phase Shifter

1.1.1 Ferroelectrics and the Phase Shifter

Ferroelectrics are crystals that electrically polarize under the influence of a strong electric field. Ferroelectricity is analogous to ferromagnetism in ferromagnetic materials. When the external electric field is removed, some of the crystals in the substance retain their polarization. If enough of the crystals have done so then the mass as a whole retains an electric polarization. If a field were applied in the opposite direction, with the intent of reversing the bulk ferroelectric's polarization, then energy would first have to be expended in reversing the previously biased crystals before the bulk material as a whole could be polarized. This behavior manifests itself as hysteresis in the ferroelectric material. Once the bulk substance is polarized it saturates. Any further increase in the

external electric field results in no further of an effect, much like saturation in a magnetic core. It is this hysteresis, the retention of electric polarization, which is characteristic of ferroelectrics [3]. Ferroelectrics are excellent dielectrics, with dielectric constants in the hundreds for many crystal types. When a ferroelectric crystal is heated past its Curie temperature (a temperature unique to each particular crystal), it enters the paraelectric region and becomes non-polar because the crystal cell assumes a symmetrical shape. Also at this temperature, the dielectric constant increases to the thousands. When the crystal cools through its Curie temperature, it (and the bulk material specifically) forms Weiss domains. Typically in the bulk ferroelectric material, groups of crystals form regions which behave as a single crystal. Known as Weiss domains, these can exist with their own distinct polarizations, even uniquely so from the polarization of the bulk material [3]. Weiss domains exist with random orientations in bulk material and only a high strength static electric field will align most, but not all, with a net polarization. Application of an electric field also has the effect of varying the dielectric constant; this is the mechanism by which the ferroelectric phase shifter functions, and is referred to as orientational polarization. Devices incorporated on the reflectarray are thin films of the crystal Barium Strontium Titanate (chemical formula $BaTiO_3$). When a static voltage is applied, the central Titanium atom at the center of the crystal is displaced, forming a dipole, and remains so even with the voltage removed [4]. This is called ionic polarization. The ferroelectric crystal under relaxed and polarized conditions is illustrated in Figure 3 and Figure 4, respectively.

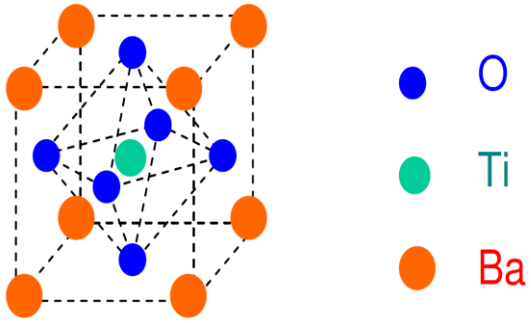

Figure 3: Crystal Lattice Cell of $BaTiO_3$

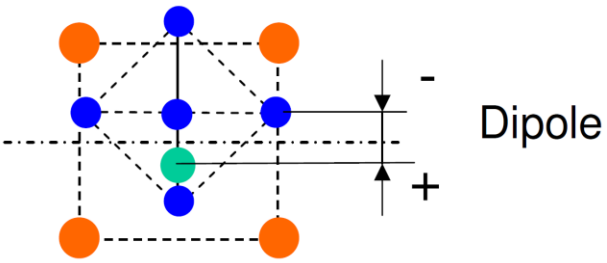

Figure 4: Deformation of Cell Followed by Polarization

The same effect is observed with an alternating electric field with the consideration that hysteresis is present. This applied voltage has the effect of depressing the dielectric constant. For the ferroelectric material to serve as an effective phase shifting element, it is made a thin film (only a fraction of a micrometer in thickness) and operated in the paraelectric region. In the paraelectric region, there exists the absence of ferroelectric domains or the practical elimination of residual polarization. This reduces the hysteresis and dielectric losses when exposed to an electric field while permitting the manipulation of the dielectric constant. It is the dielectric constant of the phase shifter that inserts phase delay in the reflected signal. By varying the applied static electric field strength (bias) to the phase shifter, the dielectric constant is varied. This variance forces a

delay upon the incident signal. When different phase shifters insert varying amounts of phase in the reflected signal, a pattern of constructive and destructive interference occurs and the resulting cophasal beam is formed. By updating the applied voltages, the beam can then be steered towards any target [2].

Given a bias voltage between 0 to 300 Volts, the phase shifters accomplish 0 to 360 degrees of phase shift, which is necessary for complete beam forming[1]. This voltage is supplied to each individual phase shifter using a high voltage bus employing a DC-DC converter and a high voltage switching integrated circuit (IC) [5].

1.1.2 Research Motivation

The motivation for researching piezoelectric transformers stems from the shortcomings of the DC-DC converter/switching IC combination. Improvements in key properties such as power consumption, speed, size, and weight can improve with this new technology. In the current implementation a DC-DC converter is used in a boost configuration that steps up a DC input voltage to reach the necessary bias voltage. While the efficiencies due to resistive (I^2R) and magnetic losses and board space cost may seem negligible, the energy and space penalties increase as more phase shifters are added to the reflectarray (which is made of 616 elements) and each require their own bias. Figure 5 is a drawing of the antenna and controller, from which, the size concerns become apparent. An eventual goal is to reduce the power draw to below 25W. Also of concern are the high

[1] The phase shifters are operated in reflect mode, not in a transmit mode. Up to 180 degrees of phase shift are achieved in each direction for a total of 360 degrees.

voltage switches. Even with using a semiconductor switching IC, the transition time (the time from one updated input voltage to a new output on the phase shifter) is too long. The transition time goal is 10μSec so as to prevent intersymbol interference. Form factor is another concern; for a ferroelectric phased array to be practically implemented, especially somewhere that size and weight are a premium, it should be light and compact, and the same holds true for the bias circuitry as well. As depicted in Figure 6, the footprint for the IC carries quite a penalty for the scale implemented on the reflectarray.

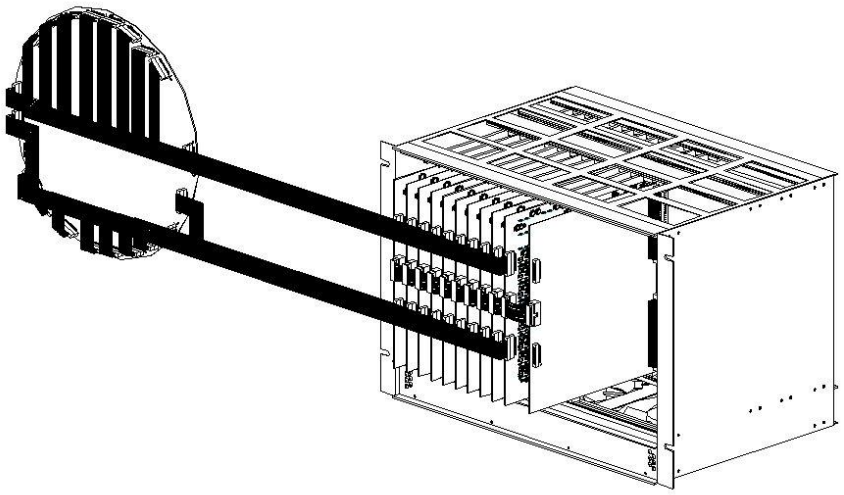

Figure 5: The 616 Element Reflectarray Controller Connected to the Reflectarray

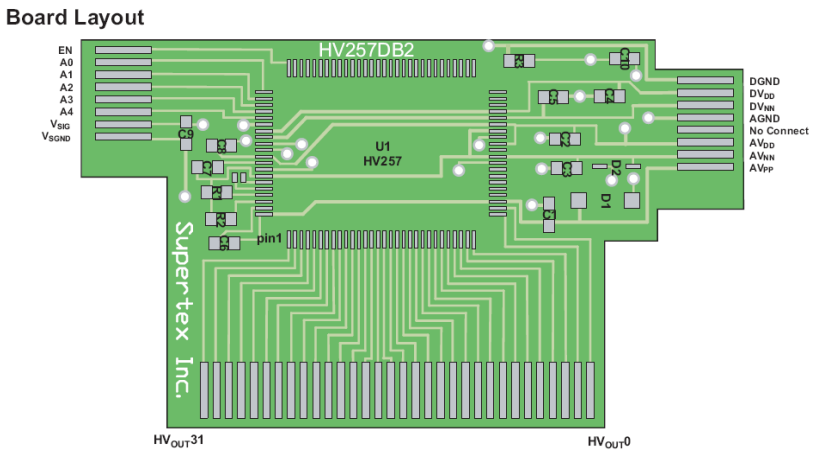

Figure 6: Element Controller with High Voltage Switching IC

This research explores the potential of the piezoelectric transformer (PT) as a fundamental component in the voltage supply for a ferroelectric phase shifter. While the previous power supply relied on magnetics in a DC-DC converter, this supply utilizes piezoelectrics in an AC-DC converter. By virtue of the piezoelectric and reverse piezoelectric effects, piezoelectric transformers succeed where magnetic ones fail; however, they operate on completely different principles. Piezoelectric transformers are electromechanical and therefore generate no electromagnetic interference. They also have higher efficiencies and higher power densities than magnetics.

1.1.3 Piezoelectrics and the Piezoelectric Transformer

Piezoelectricity was discovered by Pierre and Jacques Curie in the 1880s while studying the crystalline properties of quartz, tourmaline, and Rochelle salt. The Curies discovered that a certain class of crystals deform in the presence of an electric field (now known as the piezoelectric effect) and, conversely, develop an electric charge while being

mechanically stressed (the inverse piezoelectric effect). It was not until World War II that practical application of piezoelectrics finally caught on, first with the use of Quartz crystal oscillators in the frequency control of radio communication circuits. The twentieth century saw the implementation of ceramic-based piezoelectrics such as lead metaniobate, barium titanate, and lead ziconate titanate. Since then, piezoelectrics would find use in a myriad of industries with applications as actuators, ultrasonic transducers, sensors, and electrical filters [6]. Piezoelectrics are a subset of ferroelectrics but, what makes them unique is that the crystals' unit cells lack a center of symmetry. Piezoelectric crystals retain an electrical polarization after being exposed to an external electric field, as shown in Figure 7.

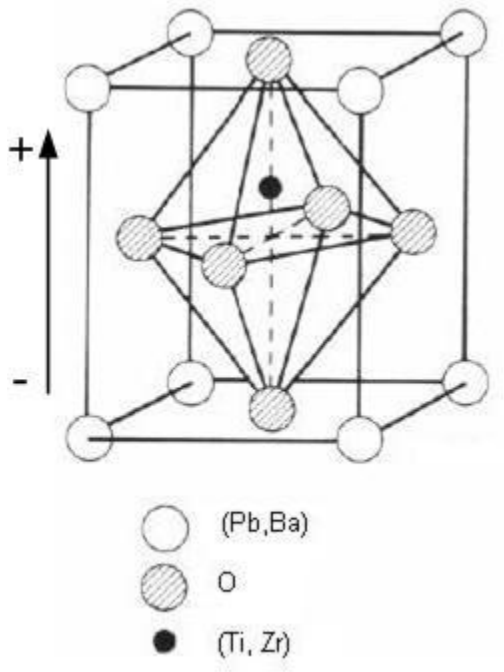

Figure 7: Lead Zirconate Titanate Elementary Cell

The remnant polarization gives the crystal the piezo and reverse piezoelectric effects. Just like the aforementioned ferroelectrics, piezoelectrics are useful in bulk form,

but, also like ferroelectrics, bulk piezoelectrics form Weiss domains. Piezoelectrics become amorphous about the Curie temperature and it is only below this that Weiss domains form [3]. For the bulk substance to function uniformly, all of these domains (and therefore their individual dipoles) must be first aligned. If they are, the entire bulk substance behaves as one giant unit crystal. This alignment, known as poling, is achieved by applying a large, static electric field to the raw piezoelectric substance.

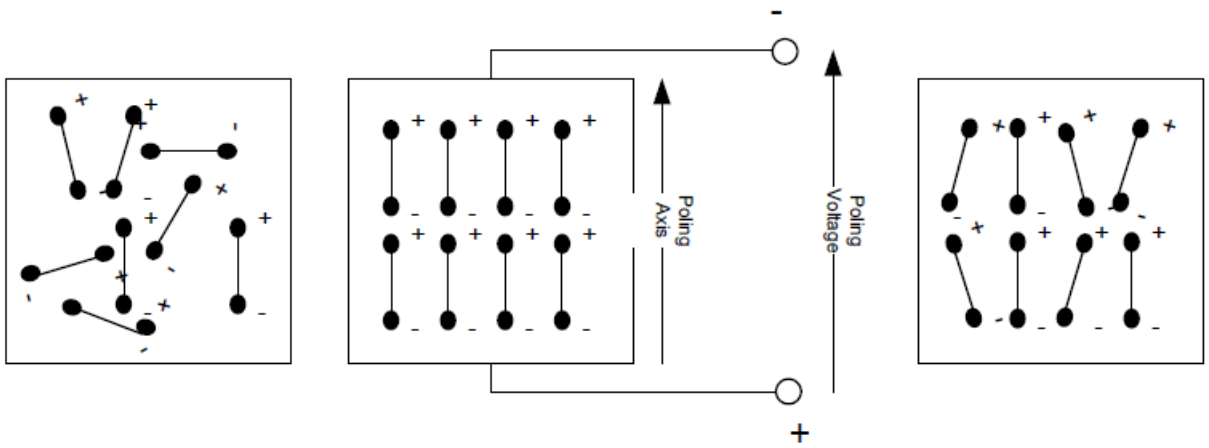

Figure 8: Piezoelectric Poling in Weiss Domains

Figure 8 illustrates how the dipoles align themselves to the external field when a voltage is applied to the now poled piezoelectric. With nearly every crystal in the field doing this, the result is a mechanical distortion in the direction of the field. It does not take a leap of the imagination to realize that when an alternating electric field is applied to the sample, the result is an alternating (oscillating) motion in the crystal.

Because a piezoelectric crystal is a bulk device that is poled, it is now anisotropic. Its behavior and properties are vector quantities in three dimensions and are referenced to the original axis of poling and the applied electrical or mechanical stresses. To assist in conveying this information, a coordinate system is used where the direction of positive

polarization is the z axis and serves as the reference. Referring to Figure 9, the x, y, and z axes are represented by the numbers 1, 2, and 3, respectively. Forces or voltages applied (or resulting) parallel to these directions are described by these numbers. Shearing about the x, y, and z axes are described by the numbers 4, 5, and 6, respectively. Radial forces or one applied to the whole surface, such as hydrostatic ones, are assigned the letter p [7].

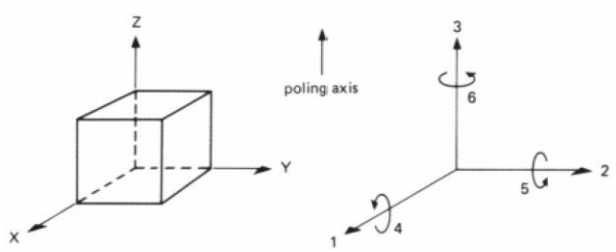

Figure 9: Designation of the Axes and Directions of Deformation

To understand why performance metrics are used and necessitate a coordinate system, it is first important to take a closer look at piezoelectric and reverse piezoelectric actions. First, consider the case of applied voltage. This voltage is described by one of the seven (the six shown in Figure 9 plus the p designation) coordinates indicating how it is applied relative to the direction of poling. If the applied voltage is parallel to and is the same polarity as the poled axis (three) then it is described by the number three and the resulting expansion is in the poled axis direction and is also described as being in the three direction. Applying a voltage in the same direction but in the opposite polarity of the polled axis results in a constriction in the poled axis direction but all resulting changes are described as being in the three direction. For forces or voltages perpendicular to the axis of poling, the applied stimulus is in either x or y direction and is described as being one or two, respectively, but with the results occurring in the three direction. The p

is assigned in special cases where the piezoelectric material experiences stresses to a plane or entire surface [8]. This nomenclature is practically assigned to simple geometric shapes like discs and plates but becomes somewhat complicated and impractical for more complex geometries; however, it is very useful in understanding the behavior of these materials and helps in understanding the functioning of the piezoelectric transformer.

Because piezoelectrics are anisotropic, their constants are tensor quantities described using the aforementioned coordinate system. The constants are a measure of the various properties of piezoelectrics and relate the interactions and directions of applied and resultant stresses, and electric fields. Some constants are expressed with two subscript indices, each referring to the direction of the related quantities, while others apply to the piezoelectric substance's chemical and electrical properties and are unrelated to the polarization [6].

Permittivity, or dielectric constant, is the dielectric displacement per unit of electric field and is expressed as ε_n^m, where m can either be a T, indicating a condition of constant stress, or an S, indicating a condition of constant strain. The n indicates which axis the applied electric field is perpendicular to.

The compliance is a measure of strain produced per unit stress and is reciprocal to the modulus of elasticity or Young's Modulus. It is expressed as s_n^m, where m is either E, indicating a constant electric field, or D, for constant electric displacement. The n is the direction of compliance for a strain in a particular direction.

The piezoelectric charge constant quantifies the effects of charges generated within the piezoelectric material. It either defines the polarization per unit of applied

stress or strain per unit of the applied electric field and is indicated using d_{mn}, where m is the direction of applied (or generated) electric polarization due to generated (or applied) mechanical strain, respectively.

The piezoelectric voltage constant, indicated by g_{mn}, is the electric field generated in the m direction per unit stress in the n direction. Alternatively, it is the strain induced in the n direction due to an applied electric displacement in the m direction.

The electromechanical coupling coefficient, k_{mn}, is a measure of how well the piezoelectric material converts electrical energy into mechanical, and vice versa. The first subscript, m, indicates the direction which a voltage is applied and the second, n, indicates the direction along which the mechanical energy is applied or developed.

Other values included on piezoelectric materials datasheets might include the Curie temperature, density, and dielectric loss factor, to name a few. An example of manufacturers' data for piezoelectrics is given in [9]. However the voltage constant, charge constant, and electromechanical coupling coefficient are the most commonly used for evaluating the performance of a particular piezoelectric.

These constants are applicable to both static and dynamic forces and fields. A piezoelectric ceramic exposed to an alternating electric field will vibrate at the drive frequency, and the same ceramic, mechanically oscillating, will produce an alternating electric field. The directions of these produced oscillations are dependent on the directions of poling and applied stimulus. From the physical characteristics of the material, every ceramic element has a particular resonant and anti-resonant frequency where, depending on the drive frequency, there is a point of either low or high

impedance, respectively. At the resonant point, the behavior is modeled with an equivalent circuit [9].

The equivalent circuit values are determined by the ceramics' material properties and dimensions, C_m models the elasticity, L_m is determined by the mass, C_o is the output capacitance between the surface electrodes and leads, and R_m models the mechanical losses in the device [8]. So for a given rectangular piece of piezoelectric ceramic operating in the transverse mode (poling direction orthogonal to the direction of applied field), there is a corresponding value for k_{31}, d_{31}, and g_{31}, which in turn, determine the equivalent parameters at resonance. The "at resonance" part should be regarded as a caveat because the equivalent circuits neither accurately reflects the piezoelectric's neither off-resonance behavior nor its nonlinear characteristics [7]. Fortunately for most at or near resonant applications, the model is sufficient. R_m, a model for the mechanical losses, plays a prominent part in determining the quality factor, Q_m, for the piezoelectric device, because at resonance, mechanical losses are greatest, whereas dielectric losses are minimal. The second source of losses are dielectric losses, they determine the electrical quality factor, Q_e, and are a maximum at off-resonance.

The first piezoelectric transformer was invented by Charles A. Rosen in 1954. He coupled two piezoelectric elements together, one an input and the other an output, in what is known today as a Rosen-type piezoelectric transformer, an example of which is depicted in Figure 10. When the input piezoelectric is driven by a sinusoidal voltage, it begins to oscillate mechanically at the same frequency. This, in turn, mechanically vibrates the second half at the same frequency, creating a sinusoidal voltage on its output. Through a combination of the piezoelectric and inverse piezoelectric effects, Rosen

realized a way to transfer energy using an electrical to mechanical and back to electrical approach, and by varying certain properties as well as the driving signal he could also vary the output to input voltage ratio [10].

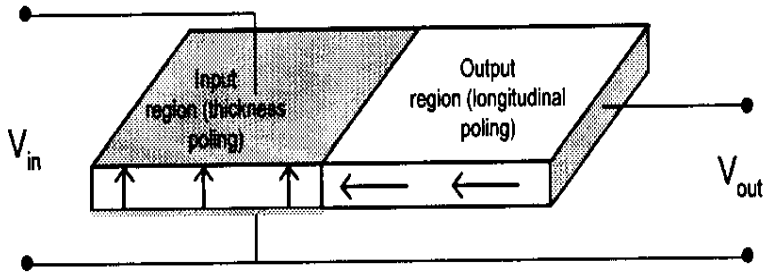

Figure 10: A Rosen-type Piezoelectric Transformer

So while the functionality is similar to a traditional transformer, the process by which the voltage step-up or step-down occurs is entirely different. As mentioned before, the piezoelectric transformer is a resonant-operated device, with the largest dimension of the device determining the lowest resonant frequency [10]. The PT's characteristic resonant frequency is a result of its length and the standing waves generated within it. The sinusoidal input and sinusoidal output generate a standing wave along the length of the device. When the wave is proportional to the device's length, there are nodes (areas of greatest displacement) and anti-nodes (areas of least displacement). At the fundamental frequency, the areas of greatest displacement are at a maximum and the whole node (or nodes) fit on the length of the device [10]. So for Rosen-type piezoelectric transformers, the drive frequency is proportional to half the device length. Because of the proportionality of drive frequency to device length, the nearer the drive frequency is to the resonant frequency, the greater the mechanical displacement is which

corresponds to greater voltages generated. Multiples of the resonant frequency will also work but not quite as efficiently as the fundamental frequency. Other frequencies, both harmonics of the drive frequency and others, increase the likelihood of other vibration modes [10]. These other modes are vibrations propagating in the transformer but only serve to dampen efficiency by diminishing the fundamental. The piezoelectric transformer acts like a highly selective, band-pass filter. So perhaps if instead of driving it with a sine wave, a square or saw tooth wave were used instead, then the PT would trap those frequencies not at the resonant frequency and only that signal at the resonant frequency would appear on the output. However, the other frequencies would likely increase inefficiency through mechanical losses by inducing destructive modes of vibration in the transformer, dampening the main mode, or increasing dielectric losses.

Figure 11 shows the accepted standard equivalent circuit model for a piezoelectric transformer [7]. Chapter three is devoted to the further analysis of the equivalent model. It allows engineers to analyze the device for practical purposes, but due to the non-linear nature of piezoelectric transformers, it is only applicable around the resonant point. The input and output static capacitances between the device terminals are modeled by C_{in} and C_{out}, respectively. The device resonance is modeled by L and C while R models the mechanical dampening. Typically, a transformer is used to model the voltage transfer ratio for the PT, but because the dielectric does not conduct current, some researchers suggest modeling the gain with dependant voltage and current sources [11].

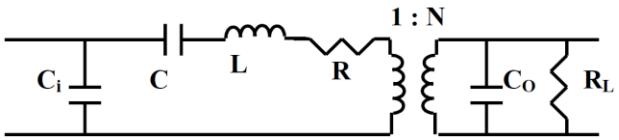

Figure 11: Equivalent Circuit Model for the Piezoelectric Transformer

Because of the PT's non-linear nature, the equivalent component values are dependent on operational and environmental conditions such as electric fields, mechanical stress, temperature, aging, and depolarization [10]. Non-linear behavior is exacerbated when the transformer is operated with large electric fields present due to the great mechanical deformation and increased losses [12]. Because the transformer's performance depends on vibrations from a standing wave, mounting the device is of critical concern [10]. It must be done in such a way that does not dampen the vibrations, so typically what is done is the device, particularly the Rosen-type transformer, is fastened to a cradle at a nodal point. This point should be the portion of the PT experiencing very little mechanical displacement due to the standing wave transferring energy from input to output. A soft and flexible material is the best choice to use in fastening the PT to the cradle because it minimizes any detrimental mechanical dampening. For research purposes, a Rosen-type piezoelectric transformer manufactured by Steiner & Martins, Inc. of Miami, Florida is used. The SMMTF53P2S40 is a multilayer, Rosen-type device made of lead zirconate titanate. From the manufacturers, the equivalent circuit data is given as such: C_i is 120nF, C is 8.8nF, C_o is 18pF, L is 1.24 mH, R is 0.5Ω, and N is 40 [13]. The piezoelectric constants for this particular device are shown in [14]. The device consists of a rectangular piece of ceramic material with a differently poled input and output half and vibrates along the length of the device [15].

For this reason it is referred to longitudinal mode vibration and the resonant frequency is proportional to this length.

Table 1: Characteristics for the SMMTF53P2S40 Piezoelectric Material

Characteristics of Multilayer Piezoelectric Ceramic Materials

Item	Unit	Symbol	SMTML	SMTAK
Electromechanical coupling coefficient		K_p	0.62	0.50
		K_{33}	0.70	0.66
		K_{31}	0.37	0.27
Frequency constant	Hz • m	N_p	2200	2130
		N_{33}	1500	1460
		N_{31}	1700	1680
Piezoelectric constant	$\times 10^{-12}$m/v	d_{33}	290	480
		d_{31}	-140	-210
	$\times 10^{-3}$Vm/N	g_{33}	24.3	15.1
		g_{31}	-11.5	-6.4
Elastic constant	$\times 10^{10}$N/m^2	Y^E_{33}	7.0	6.1
		Y^E_{11}	8.4	6.4
Poisson's ratio		σ^E	0.27	0.42
Mechanical quality factor	-----	Q_m	2000	70
Dielectric constant	@1KHz	$\varepsilon^T_{33} / \varepsilon_0$	1300	3200
Dissipation factor	%@1KHz	tan δ	0.5	2.5
Curie temperature	℃	T_C	290	210
Density	g /cm^3	ρ	7.9	7.9

All measurements made according to IEEE standard on piezoelectricity, 176-1987

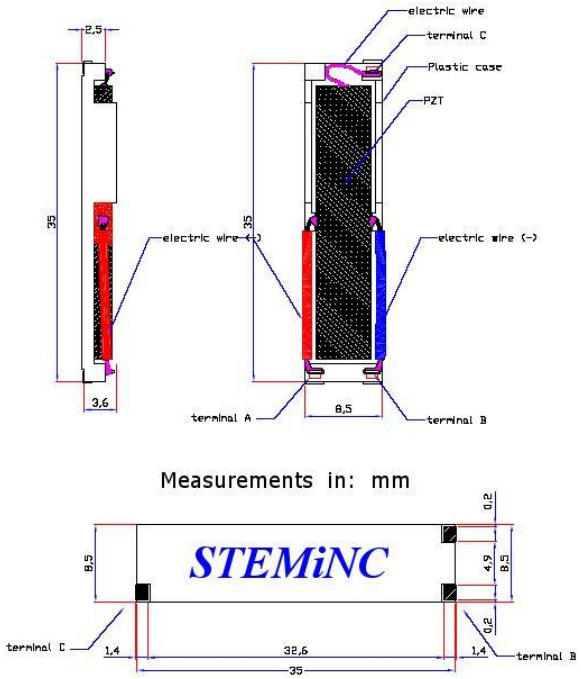

Figure 12: Mechanical Drawings for the SMMTF53P2S40 Multilayer PT

Such devices are most suitable for high step-up voltage applications due to their characteristically large gains and high output impedance [10]. The input section of the SMMTF53P2S40 operates in the transverse mode and its function is described by the piezoelectric constant k_{31}, meaning that its poling, applied electric field, and mechanical displacement are all orthogonal to one another. The output half operates in the longitudinal mode, k_{33}, where the poling, applied electric field, and mechanical displacement are all parallel to one another. Electrodes are attached using a conductive epoxy and placed respective to the devices' poling. Figure 12 is of the mechanical drawings for the multilayer piezoelectric transformer, provided by Steiner & Martins. Everything from electrode placement to footprint is clear and it is important to take note of how much greater the length is compared to the width or thickness of the device, as this is what determines the mode of propagation. Knowing the polarization from the

provided piezoelectric constants and observing the electrode placements on the device indicates the electrical and mechanical displacement within the transformer's length. The mechanical drawing also depicts an effective means of mounting the device: by using a cradle that is attached to the PT at a node using a soft material and to the electrodes using flexible conductor, so as to not dampen the device's vibrations.

The primary characteristic that makes the Rosen-type PT function so well at high voltage step-up is that its entire length is so much greater than either its width or thickness. This assures that a standing resonant wave is at its greatest size for the device and exerts maximum mechanical displacement, and therefore resulting in minimum losses, and maximum electrical stress. Due to the output half operating in the longitudinal mode (the most effective) the step-up gain is much higher [10]. Another part of the SMMTF53P2S40's design that allows it have such a high voltage gain is that it is made using multilayer construction. Instead of the input and output halves being made of bulk piezoelectric material, they are instead made of layers of piezoelectric ceramic with a thin metal conductor sandwiched between them. The first benefit to this is that it increases the total surface area and volume of piezoelectric ceramic, allowing more charge accumulation and consequently, higher voltages to be achieved [12]. The second advantage to multilayer construction is the improved thermal conductivity, which if poor, leads to detrimental effects on PT performance [16].

1.2 Problem Formulation

It is the focus of this work to explore and develop a proof-of-concept driver circuit for a ferroelectric phase shifter based on piezoelectric transformer technology. The piezoelectric transformer is but one part in a bias circuit for controlling the ferroelectric phase shifter. In order to successfully replace the current high voltage switching circuitry, the developed circuit must be able to step through 0 to 300 Vdc, be lightweight and compact, and draw as little current as possible.

With these improvements, the hope is that phased array antennas become a more practical option for engineers, particularly on space platforms. Two phased arrays were ever flown on NASA missions: an X-band array on the EO-1satillite and an X-band array on board the MESSENGER space probe. Despite being attractive from a performance viewpoint, cost and efficiency continue to curtail the greater widespread use of phased arrays.

The first step in developing the phase shifter driver circuit is to study the piezoelectric transformer itself. Because the prime motivation for developing this technology is for a space based phased array, it is necessary to evaluate the PT's behavior to cryogenic temperatures. We know the upper thermal limit of the device is the Curie temperature. This is the temperature where the piezoelectric material loses polarization and ceases to exhibit piezoelectric behavior,. The successful operation of the phased array depends on phase shifters driven by a PT-based circuit, so it is important that the driver circuit be reliable under all conditions, especially ones as dynamic as space. With

cryogenic data at hand, further design considerations can be made to accommodate for the low temperature effects of the PT's performance.

Since the piezoelectric transformer's performance is frequency sensitive, it is necessary to extract the frequency response of the gain and both input and output impedances from each device under test. While the ferroelectric phase shifter is itself a negligible load, approximated by a resistor in the tens of Megaohms, other components could have unforeseen effects on the PT. Once the peculiarities are better understood, driver circuit design and evaluation can begin.

1.3 Thesis Organization

This thesis is laid out so as to illustrate the steps taken that led to a successful proof-of-concept ferroelectric phase shifter driver circuit. In chapter one, an introduction to the technologies presented is given. The underlying principles of piezoelectrics, and the piezoelectric transformer in particular, are explained and should give the reader a thorough understanding for the material that follows. Chapter two focuses on the piezoelectric transformer and its operating characteristics with a particular focus on the frequency response and device loading with consideration given to nonlinearities. The devices' behavior at cryogenic temperatures will also be explained. The driver circuit engineering is explained in chapter three. It covers the circuit topology and theory of operation, component selection, troubleshooting, and performance results. Attention is also given to power consumed by the circuit. Modeling is an important tool as it

highlights a system's properties and behavior. Chapter three explores the equivalent model, compares it with the experimental response, and employs it in determining the equivalent circuit parameters. Chapter four provides results for the new integrated phase shifter circuit. In this section, the circuit is evaluated on how well it meets the design criteria. While the fundamental goal remains achieving significant phase shift at Ka-bands, this thesis also explores different techniques for adjusting the phase shifter's bias voltage.

As with any prototype, there are bound to be shortcomings, especially in a circuit with non-linear components. The research's conclusion makes the case for successful future work by examining those shortcomings in the driver circuit and discussing its actual implementation onto the ferroelectric reflectarray antenna. In doing so, potential solutions are offered to improving its performance and making it more practical for actual use.

CHAPTER II

CHARACTERIZING THE MLPT

2.1 Motivation

From chapter one, the underlying principles of piezoelectrics and piezoelectric transformers are given with an emphasis placed on the electrical-mechanical-electrical exchange. However it is critical to focus on a detail only briefly touched upon, that the piezoelectric transformer is a non-linear, resonant device. Despite being modeled by a second order circuit, the equivalent circuit model only approximates the PTs behavior for a limited set of operating conditions. The resonant components modeling the frequency response, as well as the transformer modeling the gain, are themselves dependant on the piezoelectric material constants. For a given set of operating conditions and a limited bandwidth of operation (around the resonant point), a PT closely resembles a high Q factor, second order system. A piezoelectric transformer is a dynamic system whose parameters change under environmental conditions and load.

Therefore, to more effectively utilize the device, especially under the conditions of desired operation, characterizing the behavior of the PT is necessary. To that end, it is important to determine the frequency response and impedance of the device over a range of temperatures especially since the ultimate application could require operation in the temperature extremes of space. The Space Shuttle payload bay experienced temperatures in excess of 170 K to 370 K, depending on attitude, payload power, and many other factors. Diurnal lunar temperatures span about 100 K to 400 K. Martian surface temperature ranges from about 130 K to nearly 300 K. The room temperature operation is a sensible place to begin since it is convenient and where the driver circuit development is taking place. From there the device is characterized at cryogenic temperatures as low as 40 K where the PT might operate in the cold of space. By observing changes occurring in the frequency response, such as a shifting resonant point, varying quality factor, or varying gain, the corresponding changes in the equivalent circuit model, and ultimately the piezoelectric constants, are deduced. Determining the frequency response is important to forming a driving scheme for the device. Seeing how it changes over temperature illustrates the design considerations that must be addressed in a final implementation of a driver circuit for a ferroelectric phase shifter based on a piezoelectric transformer. The frequency response is critical to understanding how best to drive the PT. To investigate further the effects of cryogenic exposure to the PT, laser radar mapping of the transformers' dimensions is used to look for change in device length. Any observed change would correspond to a shift in the resonant frequency. The impedance data is useful for extracting device parameters, determining how best to drive the device and understanding how it behaves in different points of operation. Using the results of a

frequency response and impedance measurement, a direct comparison is made with those at cryogenic temperatures to see what effects temperature has and infer how it changes the piezoelectric constants and in what manner.

2.1.1 Cryogenic Theory of Piezoelectrics

Piezoelectric behavior at cryogenic temperatures is explored in [17] and [18]. In [17], the author brings samples of barium titanate and lead zirconate titanate to liquid helium temperatures in a dewar and measures their coupling coefficients, frequency constants, dielectric constants, and losses. In [18], the researcher takes a more in-depth and thorough approach, analyzing various samples of PZT from -150°C to 300°C. This study also evaluates the effects of temperature on the piezoelectric coupling coefficients, dielectric constants, and losses too, with an analysis of the added thermal-mechanical effects. Both studies find that as piezoelectric ceramics become cooler, the piezoelectric charge and voltage constants and the coupling coefficient are all reduced. This indicates a decreased effectiveness in the stress-electric charge relationship of the piezoelectric material. The dielectric constant decreases over lower temperatures resulting in the piezoelectric substance having a poorer response to an applied electric field or mechanical stress. A reduction in compliance is observed, corresponding to an increase in Young's Modulus. This reduction in elasticity affects how mechanical waves propagate through the substance and is confirmed by an increase in the frequency constant. Lastly, at cooler temperatures, the piezoelectric substance becomes less lossy. All the aforementioned changes are attributed to a reduction in piezoelectric domain wall

mobility. The aforementioned works give a very good idea of what is expected from a piezoelectric-based device subjected to the deep cold of space. Since the MLPT is a more complicated arrangement of piezoelectric materials, further analysis of the cryogenic condition is necessary.

2.2 Experimental Characterization: Procedure and Results

The SMMTF53P2S40 MLPT is analyzed for the frequency response under room temperature and cryogenic conditions. To do so, a 1 Volt peak-to-peak (Vpp), sine wave is applied and swept through a series of frequencies around the devices' natural resonant frequency. To drive the PT, an operational amplifier (Op Amp) was wired as a unity gain amplifier buffering the signal from a benchtop signal generator while an oscilloscope measured the output. The driver details are left to chapter three. The frequency was swept from 45 kHz to 60 kHz in 250 Hz increments. This range is large enough that all shifts in the devices' natural and working resonant frequencies (53 kHz and 55 kHz, respectively) are observable. The natural resonant frequency is characteristic of just the piezoelectric bar (its dimensions and properties) and the working resonant frequency is a manufactured specified value for operating the device under load. The input impedance was measured using an HP4192A impedance analyzer and the magnitude and phase were recorded from 48 kHz to 60 kHz.

Cryogenic testing was done using a closed-cycle, helium-cooled cryostat. The whole setup is shown in Figure 13.

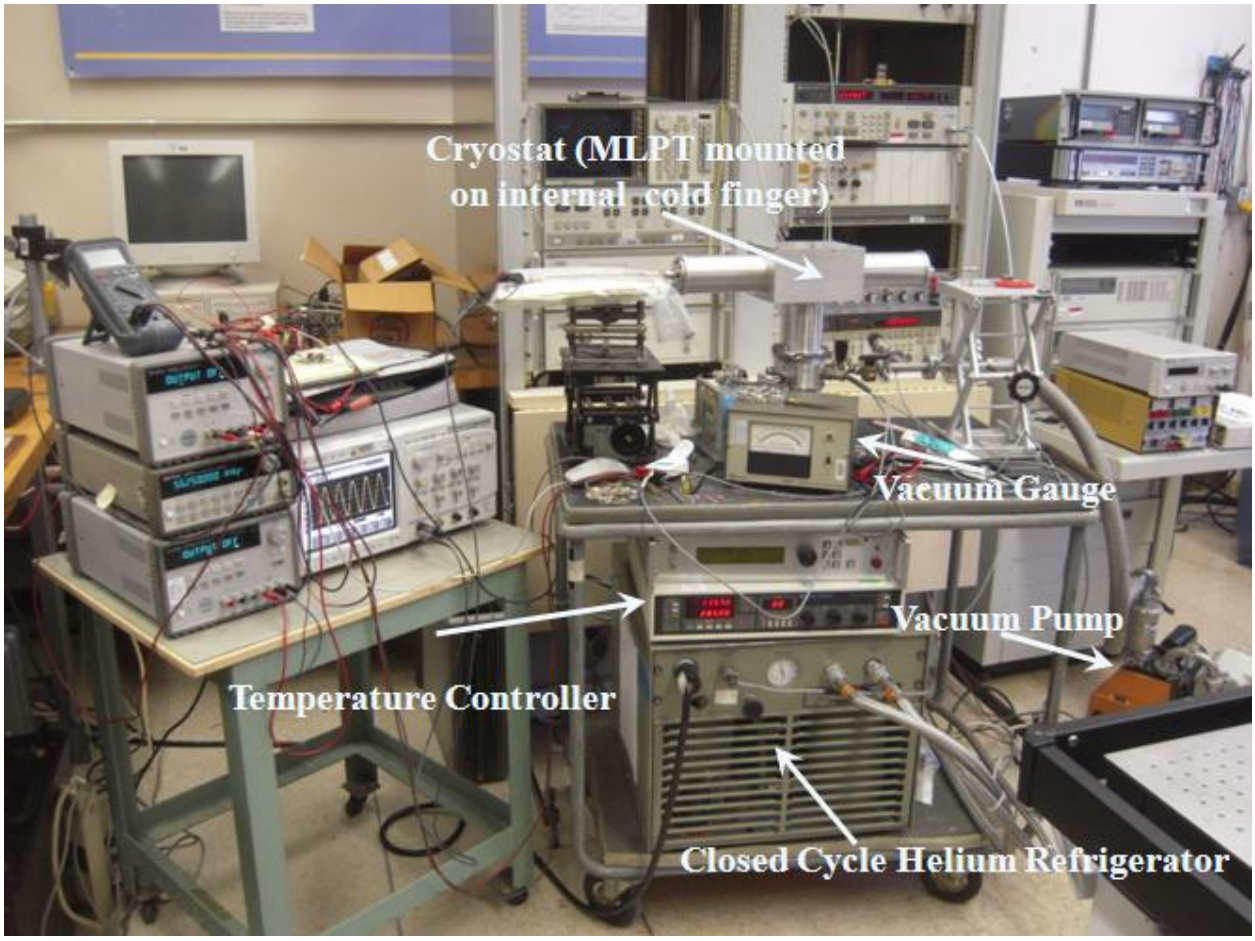

Figure 13: Cryostat and Instrumentation

The PT cradle was epoxied to a thin piece of aluminum to make handling it easier and to provide a surface for thermal contact. The Tra-bond epoxy is thermally conductive and has a low emissivity. This ensures improved heat flow. A silicon-based heat sink compound was applied between the aluminum plate and cold finger to assure good thermal contact. The device electrodes were accessed via probes into the cryostat. This also allowed the application of other sensors. Due to the thermal impedance between the cold finger and the PT (the adhesive holding the PT to the cradle, the cradle itself, the thermally conductive epoxy, the aluminum plate, and the heat sink grease), a way to

measure the PT's temperature directly was necessary. A resistance temperature detector (RTD) was epoxied, using the same material holding the PT to the aluminum plate, to the main node of the PT. At the fundamental node there is little mechanical displacement of the PT from the standing wave in it so attaching the PT should cause minimal mechanical dampening. The setup, with the PT connected to the cryostat's cold finger and wired to all the electrodes, is shown in Figure 14.

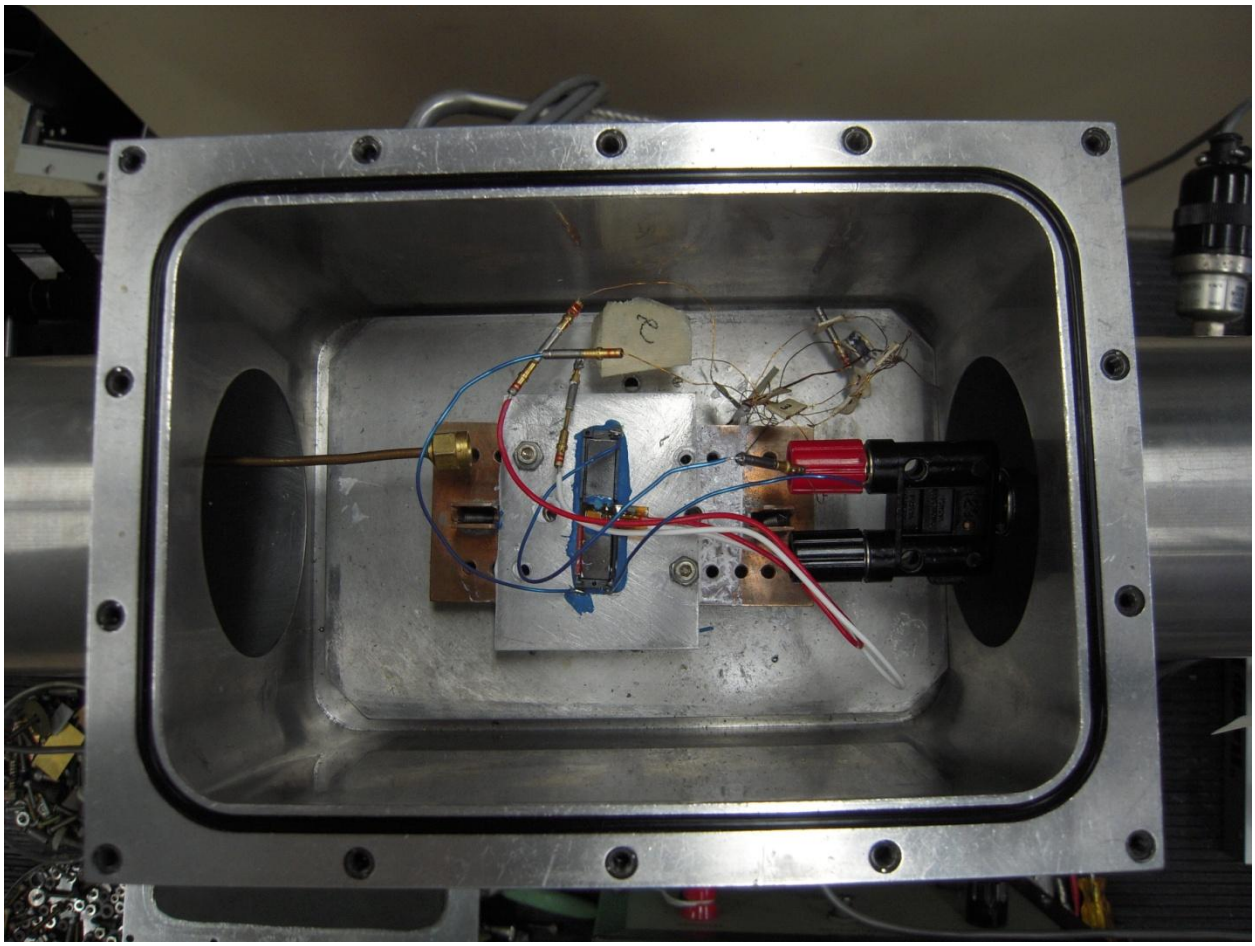

Figure 14: PT Setup for Cryogenic Testing

Frequency response can now be measured at sequentially lower temperatures of the PT.

The results for both tests are shown in Figure 15 and Figure 16. Figure 15, the PT's high Q response is observed resonant at approximately 54 kHz with a gain of 348 at room temperature (298 K). Figure 16 shows the results while the PT is in the cryostat. At 293.09 K, the device is mounted in the cryostat but it is not yet chilled down. In there, the resonant point is measured at 52.8 kHz with a gain of 322 V/V. The large shift in resonant frequency is mostly due to loading from instrumentation leads, a problem that presented itself throughout the research as different instrumentation was used. More on the effects of instrumentation loading can be found in [19].

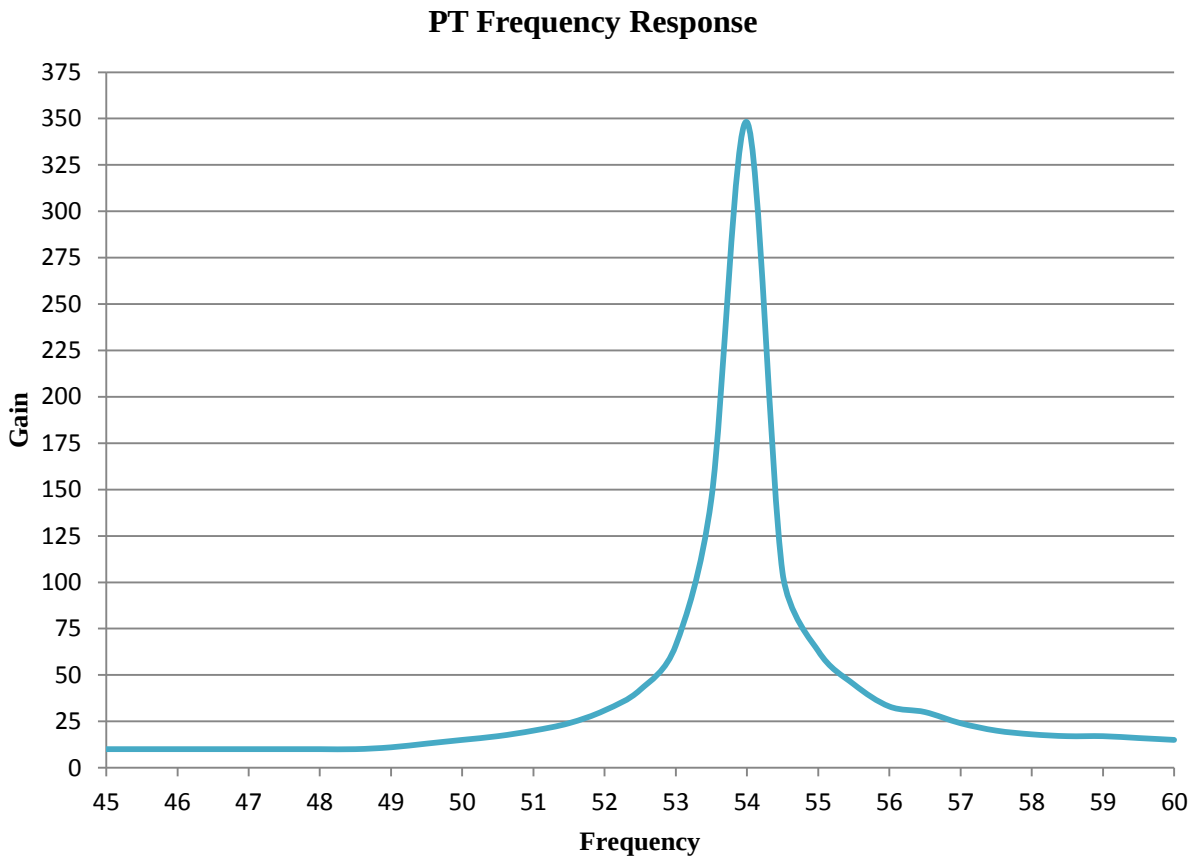

Figure 15: PT Frequency Response at 298 K

When the device's temperature is reduced to 142 K, the resonant frequency shifts to 53.8 kHz and the gain is markedly reduced as well. Repeated measurements of gain at cryogenic temperatures confirm this effect. A curious occurrence is seen in the chilled response of the device that warrants a closer look. The shape of the waveform shows a double-hump, something characteristic of dual-resonant or doubly-tuned circuits. To confirm if this phenomenon is indeed present, the frequency response is measured again at 140K (in steps of 25 Hz). The results are shown in Figure 17.

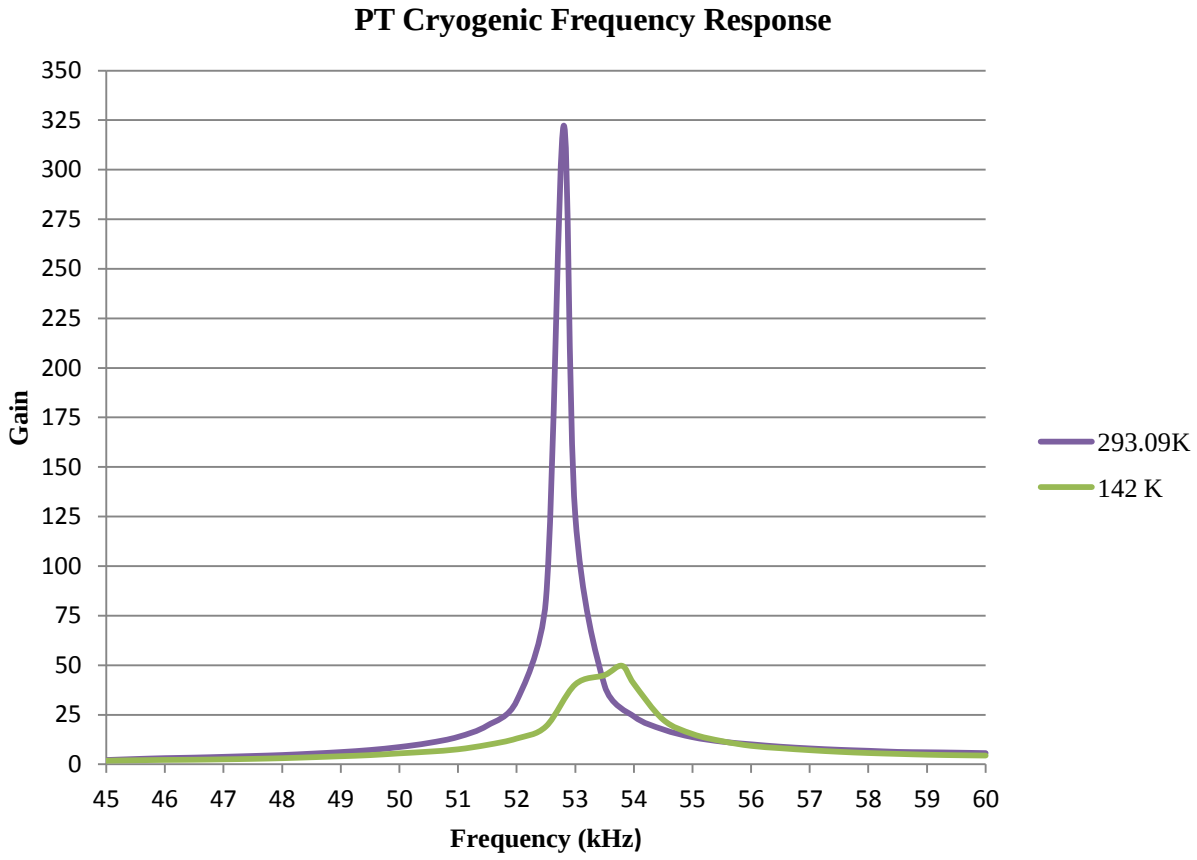

Figure 16: PT Cryogenic Frequency Response

The second test confirms the suspicion of a double resonance in the PT, with a peak at 54.9 kHz and a second peak at 56.25 kHz. The roughness in the plot is due to the

impedance analyzer's resolution not being fine enough near resonance. Split resonance occurs in systems where at two distinct frequencies, different portions of the system begin to resonate. In the case of two LC circuits that are magnetically coupled, if the coupling is strong enough, only one resonant frequency dominates. As the coupling is dampened, the two circuits are less affected by one another and resonate at their own unique frequencies. This forms the distinct double-hump shape. Exactly how this effect is manifested in the piezoelectric transformer is unclear but may be due to the cryogenic temperatures affecting the coupling between the input and output halves of the device which are both resonant devices themselves. Whether the separate resonant frequencies are due to the different polarizations or other material properties is uncertain, but the presence of a dual-resonance mode at cryogenic temperatures is undoubtedly there. The test results agree with [18], where the dampened gain and shifted resonant frequency are results of the piezoelectric material's temperature dependence. The shift in resonant frequency is attributed to variation of Young's Modulus. As in [20], researchers have made efforts to synthesize an approximate transfer function from the frequency response and equivalent circuit of the PT, however, the limitations of this approach are in its restriction to a particular point in operation.

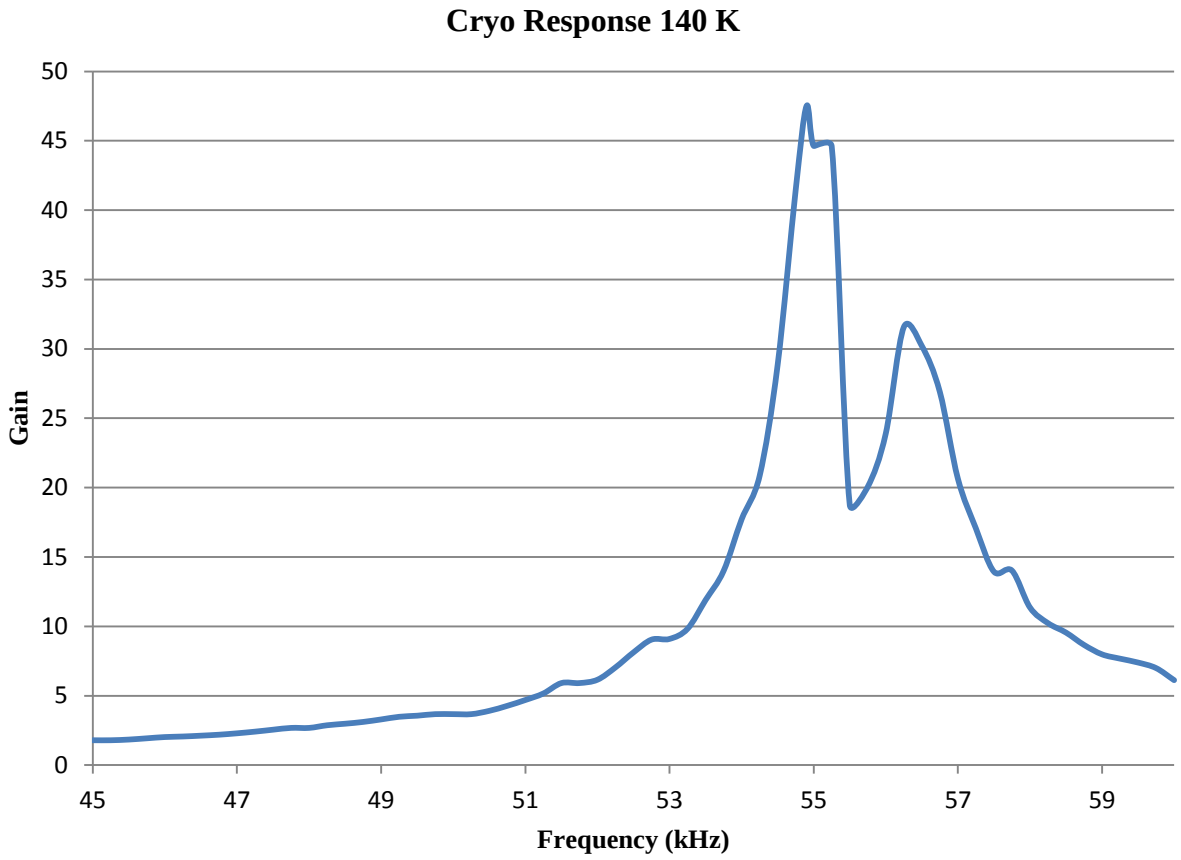

Figure 17: PT Cryogenic Split Resonance Frequency Response

For the SMMTF53P2S40, Steiner and Martins Inc. lists its working resonant frequency as 53 kHz with a variance of ±3 percent. From [21], the resonant frequency for a solid bar of piezoelectric ceramic is calculated using Eq. (2.1).

$$f_r = \frac{1}{L}\sqrt{\frac{Y^E}{\rho}} \tag{2.1}$$

Where f_r is the resonant frequency, L is device length along the main mode of vibration, Y^E is the value of Young's Modulus for the material, and ρ is the material density. Approximating the multiple layers in its construction as being thin enough to consider a solid, single piece, and assuming a single, longitudinal mode of vibration, this

equation gives the resonant frequency as 53.1 kHz. The experimentally determined resonant frequency is 53.9 kHz, which is just outside the manufacturer's tolerance for the device, the difference of which may be the effect of different measurements and instrumentation [19]. Steiner and Martins Inc. rely on IEEE Standard 176-1987 for characterizing its piezoelectric devices [22]. A modification of the procedure described in the standard is to attach a 100 kΩ load to the transformer and take readings, based on which the user can determine the devices' characteristics. However, all the measurements performed in this work are done operating in the open circuit condition (the phase shifter to be driven has an input impedance in excess of 10 MΩ) and with different instrumentation than the device manufacturer. It stands to reason then that differences in equivalent parameters and frequencies from this experiment versus the manufacturer's can be attributed to the different instrumentation and operating conditions.

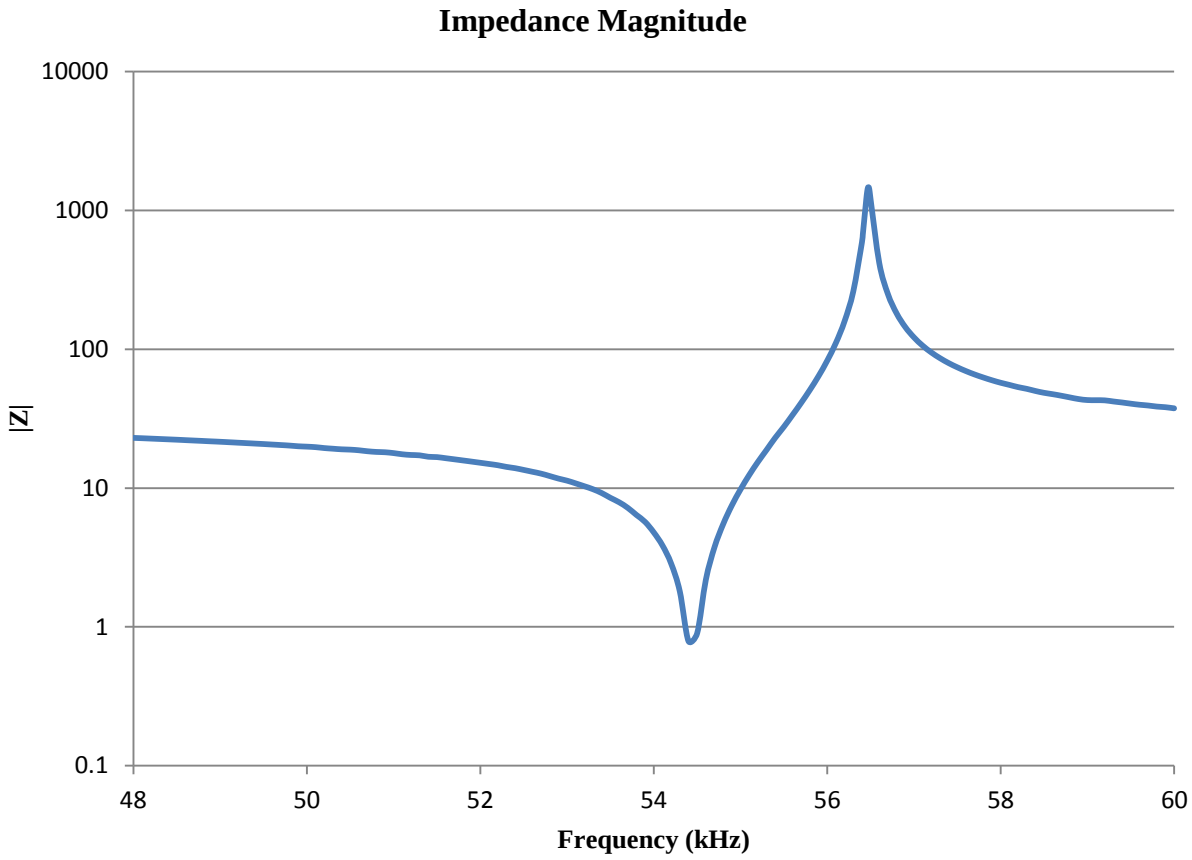

Figure 18: PT Input Impedance Magnitude

The impedance magnitude and phase for the PT help show how to best drive the device over the frequency range of operation. The device was measured open circuit to best illustrate its extreme case of operation with the phase shifter. Figure 18 and Figure 19 are the impedance magnitude and phase, respectively. The impedance is very dynamic over frequency, with both resonant and anti-resonant points and a complete 180 degree phase shift. At the resonant point, the impedance magnitude is 0.79 Ω at an angle of 0 degrees and occurs at approximately 54.5 kHz. This resonant value of the impedance is close to the manufacturer-specified value of 1.4Ω. The anti-resonant point is at approximately 56.47 kHz and is 1459 Ω at 0 degrees. The phase undergoes a complete

180 degree shift from -90 degrees to 90 degrees and back, over a 1.97 kHz span. The equivalent at-resonance circuit model for the piezoelectric transformer is a series RLC circuit. The anti-resonant frequency has an impedance represented by a parallel RLC circuit, something not included in the equivalent circuit. Exactly why this effect occurs is uncertain but it may be due to resonance in the different modes of coupling in the PT. Instead, it might be due to a difference in phase between the applied voltage and mechanical vibrations resulting in an applied anti-phase, dampening the response.

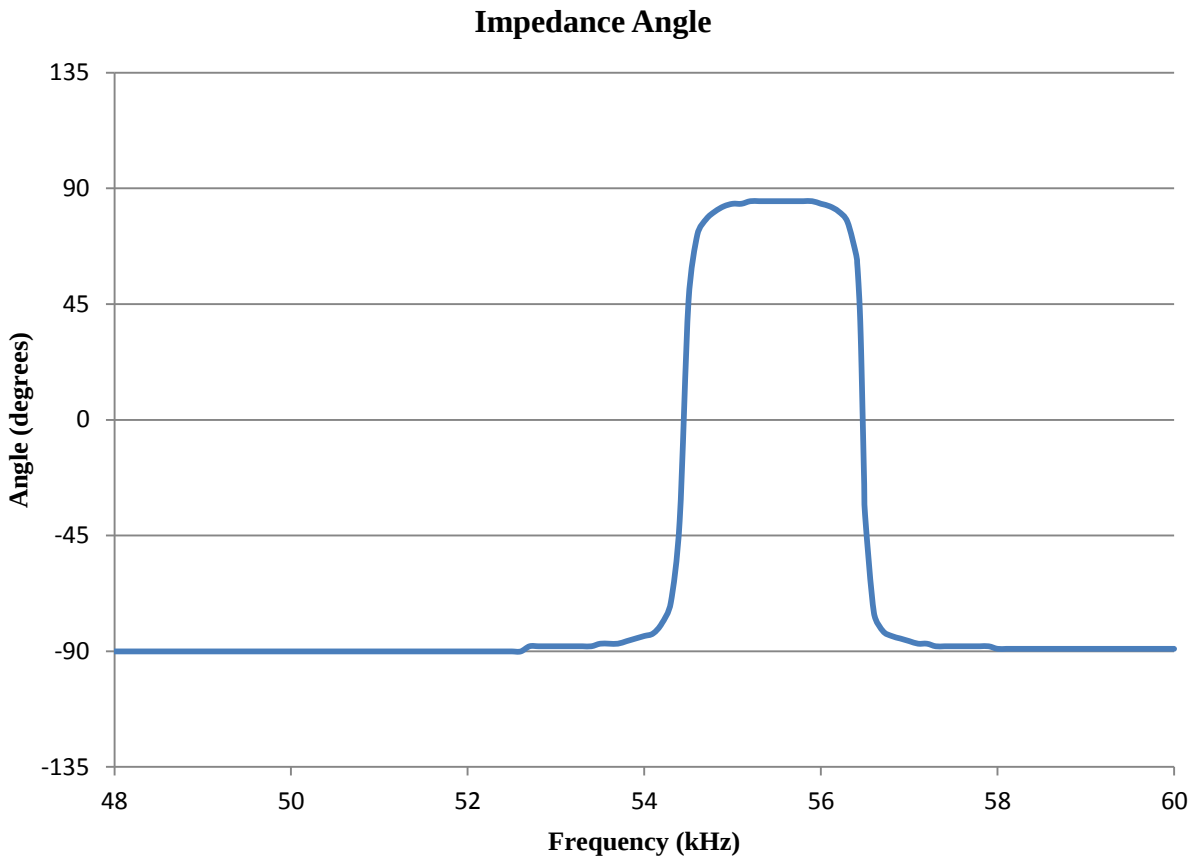

Figure 19: PT Input Impedance Phase Angle

While phase information is unnecessary for this application, it is interesting to see the confirmation of device performance by observing the impedance. From the frequency

response measurements' results, where the resonant frequency shifted higher at lower temperatures, it is plausible to assume the same effect occurs in the impedance of the device. From [17], research shows losses are reduced at cooler temperatures; therefore, the impedance at resonance drops to a new low. Referring back to Eq. (2.1), the increase in Young's Modulus correlates to a direct increase in resonant frequency. Even though the change in piezoelectric performance is attributed to temperature's effect on the piezoelectric domains, the effect of temperature on the device remains unclear. The device manufacturer includes no appropriate data for calculating the changes in length due to temperature therefore, it was necessary to try to determine it independently. An increase in resonant frequency could be attributed to a contraction of the device length because the resonant frequency is inversely proportionally to the length along which the fundamental mechanical wave propagates. Leica's LR200, shown in Figure 20, is a coherent laser radar used for surface mapping that was used to measure the distance of four fixed points on the piezoelectric transformer both before and after cooling. The relative change in distance is associated with an overall change in device length and is used to calculate the new resonant frequency.

Figure 20: LR200 Coherent Laser Radar.

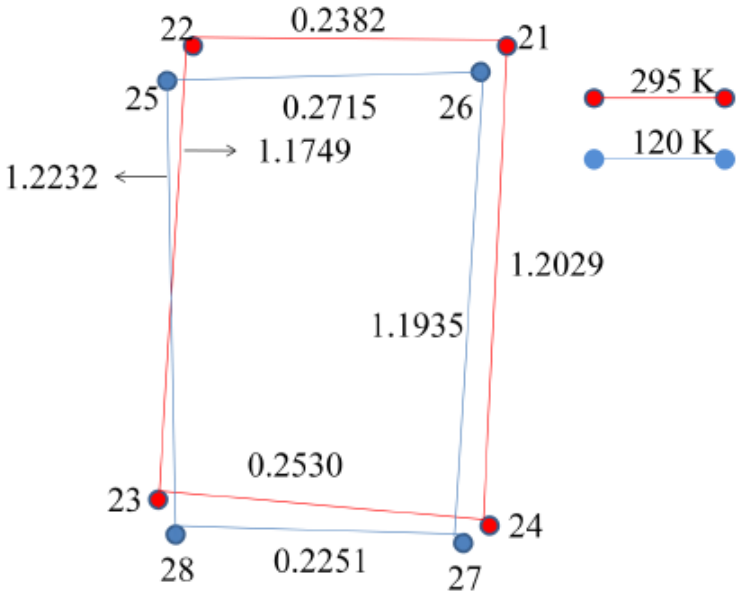

Figure 21: Dimension Measurement Results

Until now the understanding of the effect that temperature has on the resonant frequency is its effect on Weiss domain mobility. However, because the resonant frequency depends strongly on device length (ideally the device length is the resonant frequency wavelength for a Rosen-type piezoelectric transformer) and Steiner and Martins Inc. give no physiochemical data on PZT, except for the Curie temperature, there is motivation to measure for contraction (or expansion). To measure for change in dimension, a cryostat lid with an integrated calcium fluoride window was used. This window is essentially transparent to the visible spotting laser and the 1550 nm LR200 measurement laser beam. The transformer was mounted just as in the previous cryogenic experiments and using a laser radar and a series of mirrors, a spotting beam was fixed on the PT. Using spatial analyzer software, four points were selected on the device as targets for measuring any relative change in the device dimension under cryogenic temperatures. Unfortunately, a lack of precision in the spotting laser created enough placement error that the resultant measurements were inconclusive. Figure 21 is the result of this measurement; unfortunately, it also shows the lack of precision in the spotting laser that created enough placement error that the results were inconclusive.

2.3 Conclusion

From the test results, a number of conclusions about driving the PT are drawn. The frequency response shows that the necessary voltages required to bias the phase shifter can be generated from the piezoelectric transformer within a bandwidth centered

about the resonant frequency. However, at cryogenic temperatures the PT's gain drops significantly and the resonant frequency is shifted higher. Therefore, an appropriate driving scheme requires that, in order to reach the necessary higher voltages at cooler temperatures, a larger input signal is required, and because the resonant frequency shifts to larger values, the final PT driver will require some kind of frequency tracking circuitry.

The impedance shows that at resonance, the input becomes purely real and at a small value, but quickly grows to large values past the resonant point. The datasheet for the device lists the series resistance as 1.4 Ω whereas the measured value is 0.79 Ω, a difference possibly due to load dependence on input resistance. An initial assessment on efficiency was carried out by observing the current drawn by the Op Amp driver for the PT. Because external power was only delivered to this element, its current draw is a sum of the Op Amp quiescent current and the load current pulled by the PT and external circuitry. The datasheet for the OPA547T lists the quiescent current as approximately 20 mA (10 mA per supply rail) [23]. From the impedance measurement, the PT draws little current at off-resonance where the input impedance is high. As the drive frequency moves closer to resonance, the input impedance drops until it reaches a minimum, at which point the PT draws the most current. This increase shows up as an increase in current drawn by the Op Amp. From the frequency response characterization measurements at off-resonance, the Op Amp draws 24 mA and reaches 80 mA at resonance. This current increases as the PT is driven by larger and larger input voltages. The piezoelectric transformer is most efficient at resonance [24] with the bulk of the applied current creating the charge displacement that polarizes and depolarizes the

piezoelectric material. Thermal loss is dynamic and attributed to the movement of whole Weiss domains against one another. The magnitude of this loss increases at resonance but dominates the energy consumed by the PT at off-resonance. It is detected in the lab by measuring the temperature increase in the PT as the drive signal magnitude was increased at resonance, which corresponds to the greatest stresses due to the magnitude of electrical and mechanical displacements in the PT.

One of the goals of characterizing the PT is to form an idea of how it functions as a component in the driver circuit. To this end, the impedance is useful because, as seen from the impedance plot, the input impedance varies dramatically over frequency. This necessitates a signal source that can supply (and sink) ample current when necessary and rapidly enough that it does not saturate and limit the PT's performance. From the impedance plot, the piezoelectric transformer's behavior around resonance is better understood. Consider the equivalent circuit model for the PT, particularly the series RLC portion. The reactive elements model the oscillatory behavior in the device but the resistor models the dampening. The impedance plot shows a range of frequencies for which the input impedance is least (around resonance). From the frequency response, the PT's behavior starts off as a high Q system. Referring to the equivalent circuit model, basic circuit theory says a series resonant system's bandwidth is proportional to the quality factor and the Q of a system is a ratio of the resonant frequency to its bandwidth. As stated earlier, when the device is cooled, the mechanical losses, modeled as R, decrease, but so does the resonant magnitude. The drop in magnitude is far more severe than the drop in R, resulting in a decreasing Q and increasing resonant bandwidth. It is important to recall that the resonant frequency shifts higher as well. The quality factor

quantifies the energy stored in the circuit to the energy dissipated in it. Therefore, at cryogenic temperatures, the piezoelectric transformers' ability to exchange charge to strain and, vice versa, is damped. However, the shift in resonant frequency is not just unique to the effect of temperature but to loading as well ([25]), an occurrence that is well worth investigating in future research.

At the point where double resonance appears in the behavior of the transformer, the Q factor is not so clear and neither is defining it. It would not be unreasonable to assume that the same effect that is occurring to the energy exchange in the single resonant mode is also occurring in the double resonant one but future work would be required to understand how.

Where these results are most useful is in designing a driving scheme for the device. At higher temperatures where the resonant gain is large, a smaller driving voltage is necessary in achieving the desired output, whereas when the devices' temperature drops, the input voltage must increase to match the desired output. The shift in frequency requires a way to track resonance over temperature. The fact that the resonant bandwidth broadens over cooling temperature ranges might be used to an advantage. The consequences of a split resonance may be no worse than selecting just one frequency, even if it is within the resonant bandwidth but not one of the peaks itself.

CHAPTER III

PT MODELING AND SIMULATION

3.1 Overview

A system's physical model is a useful tool for implementing and developing a physical system. A good model belies an understanding of the physics operating within a device and governing its behavior. It helps engineers incorporate the physical system by giving a functional representation that designs can be based on. However, the model is only as good as the accuracy of the math behind it. Sometimes a tradeoff must be made between the fidelity of the model and the practicality of using a simpler or more complex model. Such is the case with the piezoelectric transformer. Researchers have found great success in designs based on the standard model, and if it were not for the extremes under which the transformers were subjected to in this work, the equivalent circuit might aid in the analysis of the phase shifter circuit as well. The dynamic conditions of spaceflight preclude using the linear model of the PT. From chapters one and two, the effects of environment and operation were observed for their impact on device behavior. The model

is a representation of this behavior (around the vicinity of resonance) and not the physical device; therefore, the model will not represent the physical properties of the device without some significant increase in the model's complexity. As an excellent example, there is the case of double resonance that occurs at the extremely cold temperatures seen in chapter two. Such behavior requires that the equivalent circuit have two resonant circuits that are coupled. The appendix successfully addresses the double resonance model. The manufacturer's equivalent component values are subject to change based on the operation of the device, specifically because they characterize the PT under different conditions than the ones used in this work. To produce accurate simulation results, the model must be tuned to reflect the device's behavior. In order to do this, and to run all other simulations, the equations for the PT's transfer function and input impedance must be found. Using ordinary circuit theorems and referring to the circuit schematic in Figure 11, the transfer function and input impedance are found and shown in Eq. (3.1), (3.2), and (3.3), respectively.

$$\frac{Vo}{Vi} = \frac{sR_LC}{s^3n^2R_LC_OLC+s^2(n^2R_LC_OCR+n^2LC)+s(n^2R_LC_O+n^2CR+CR_L)+n^2} \tag{3.1}$$

$$Z = \frac{R_L}{sn^2C_OR_L+n^2} + \frac{s^2LC+sRC+1}{sC} \tag{3.2}$$

$$Zin = \frac{Z\frac{1}{sC_2}}{Z+\frac{1}{sC_2}} \tag{3.3}$$

To understand how well the model can correlate with the physical system and how it differs from the natural response of the device, Mathcad simulations are compared with the PT's actual response.

This chapter is split into two sections: the first includes simulations and modeling for the device under static conditions. This means that the PT's assumed ambient temperature and load are fixed (298K and 10 MΩ, respectively) and the drive frequencies are from 45 kHz to 60 kHz, the same as conditions the device was experimentally characterized at. The results show the deviation between actual response and simulation and then the steps taken to reconcile the model to the actual device's behavior. The new equivalent parameters would then redefine the model for the actual condition of operation in the phase shifter circuit.

In the second part, the PT's behavior is simulated under dynamic conditions. The results of these simulations will show how the model behaves outside the intended range of operation and how the model compares to the physical device.

3.2 Static Operation

An accurate model gives a concrete idea of how a system functions. In the case of the piezoelectric transformer, the model replicates the high, single resonant behavior of the device. Because the model parameters are determined by the device physical properties, which are themselves subject to external conditions, those values given by the manufacturer are going to be different for the conditions under which the device is used here, specifically with an extremely high impedance load. To illustrate this point, a number of simulations are run comparing the simulated results of different sets of equivalent model component data to the experimental results. Next an attempt is made to

tune the equivalent model values so that the response matches the experimental frequency response. Lastly, a curve-fitting technique is applied in order to try and derive equivalent parameters from the device.

Figure 22 is a plot of experimental and simulated values using the equivalent component values supplied by the StemInc.

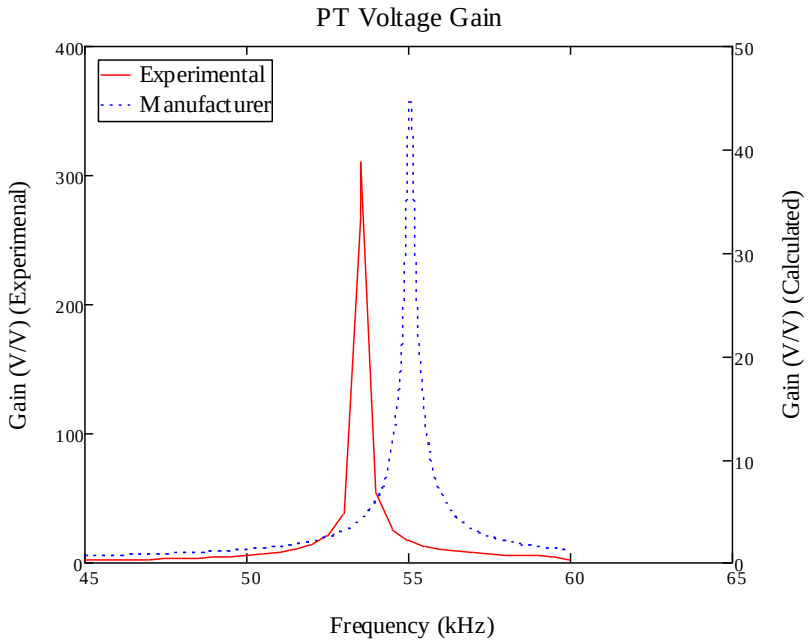

Figure 22: Experimental and Simulated (Mnfr.) Frequency Responses

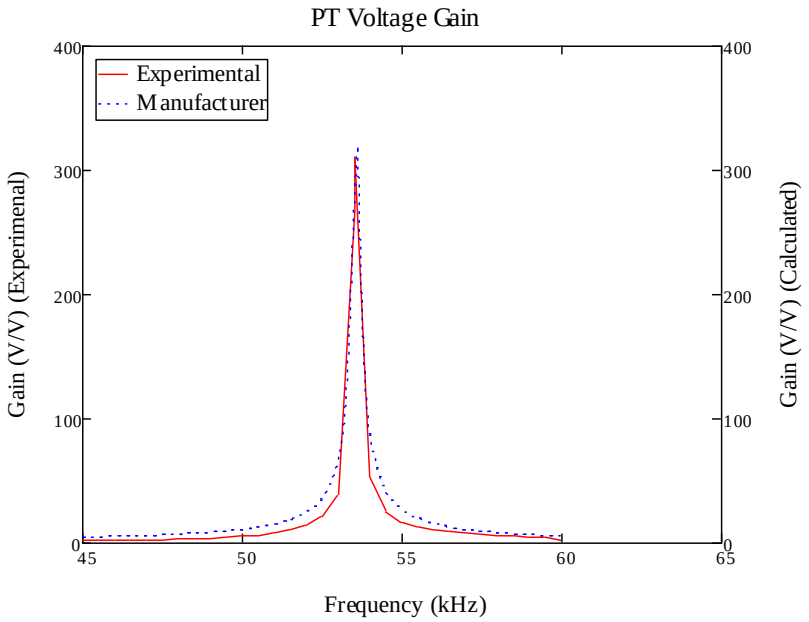

Figure 23: Experimental and Simulated (Mnfr.) Frequency Responses (Tuned)

The results show the simulated resonant frequency is about 5 kHz higher and the gain is roughly 7.5 times smaller. By iteratively adjusting the values of n and a multiplier, the manufacturer's response is brought into close agreement with the experimental. The adjusted response is shown in Figure 23.

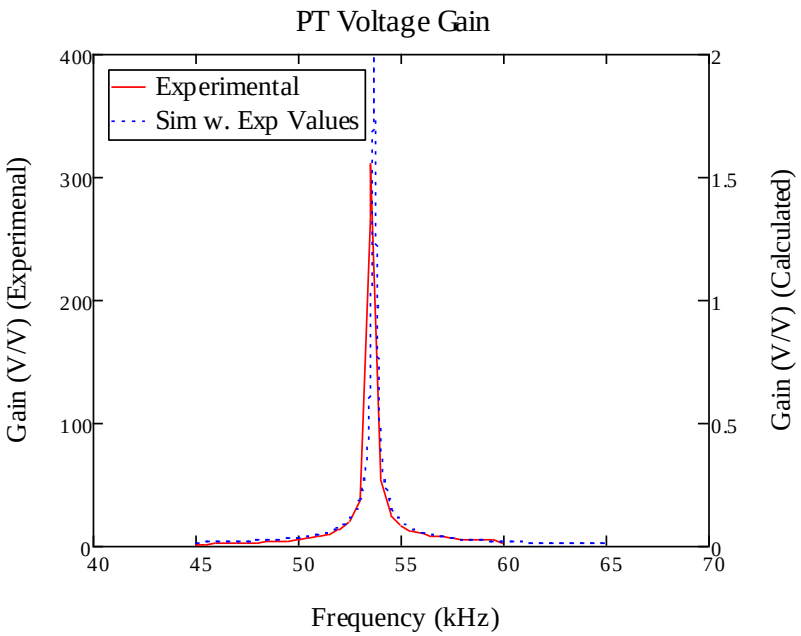

Figure 24: Experimental and Simulated (Exp.) Frequency Responses

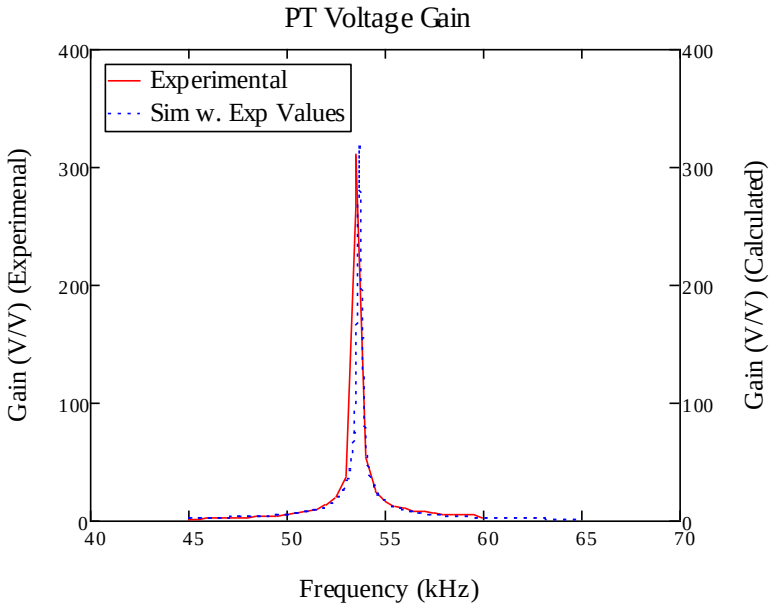

Figure 25: Experimental and Simulated (Exp.) Frequency Responses (Tuned)

The equivalent values for before and after are shown in Table 2.

Table 2: PT Equivalent Component Values

Component	Manufacturer Values	Final Values
R (Ω)	0.5	0.5
L (mH)	1.24	1.24
C_O (pF)	18	18
C (pF)	8800	8800
n	40	45.5
Multiplier	1	7.6

In the second simulation, an attempt is made to extract parameters from the experimental response in order to tune the model. From the experimental frequency response data, the resonant frequency and resonant gain are shown to be 53.54 kHz and 311 V/V, respectively. The resonant input impedance was measured as 0.79 Ω. This allows for values of LC, n, and R to be solved for. The PT equivalent circuit includes a series resonant circuit with the resonant frequency calculated by using Eq. (3.3).

$$f_{res} = \frac{1}{2\pi\sqrt{LC}} \tag{3.4}$$

Using the experimental value for the resonant frequency, the product LC is solved for and substituted back into the transfer function, shifting the resonant frequency. At resonance, the impedance for an RLC circuit is entirely real so the 0.79 Ω can be substituted for R. The resonant gain is substituted for n. The result for this simulation is shown in Figure 24. In it, the resonant frequency corresponds very well; the gain differs by a factor of almost 200. Just as with the first simulation, the second one is tuned to fit the experimental response and the result is shown in Figure 25 and the values in Table 3.

Table 3: PT Equivalent Component Experimental Values

Component	Experimental Values	Final Values
R (Ω)	0.79	0.79
LC	8.83656608236E-12	8.83656608236E-12
C_O (pF)	18	18
C (pF)	8800	8800
n	311	311
Multiplier	1	160

The last method used in determining equivalent component values is to employ curve-fitting techniques. The results are shown in Figure 26.

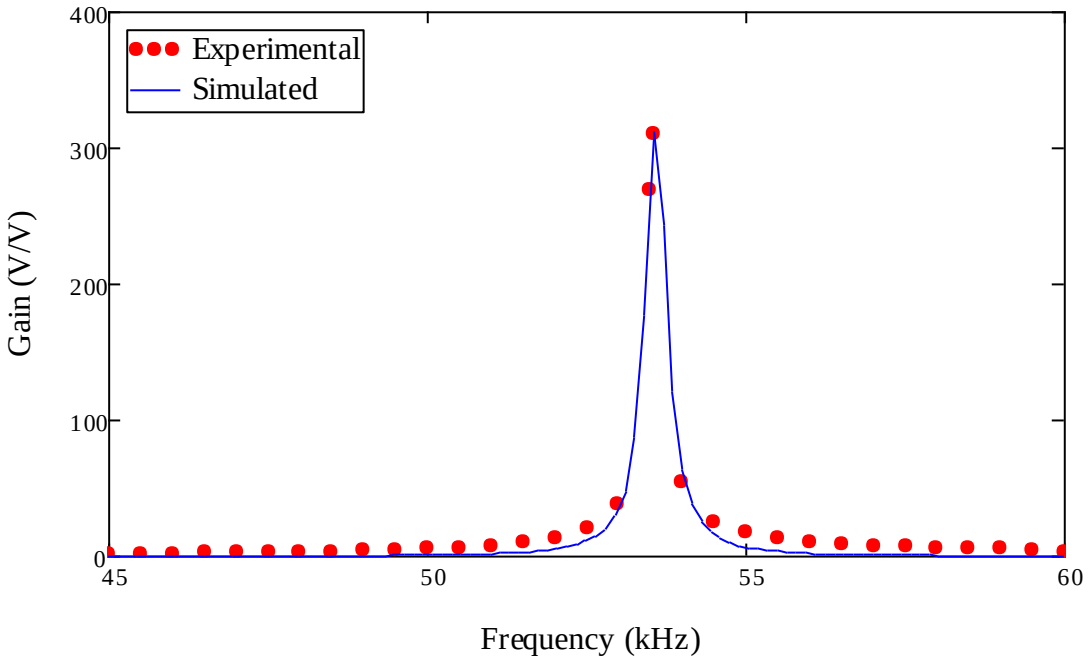

Figure 26: Curve fitting Frequency Response

By substituting the coefficients of the PT's transfer function with a generic a, b, c, d, and e, a function for the curve is used and a regression is solved for using Mathcad.

Mathcad uses the "genfit" command to apply a nonlinear, least-squares regression, fitted curve.

These values can then be set equal to the coefficients in the transfer function resulting in a nonlinear system of equations (Eqs. 3.4-3.8).

$$CR_L = 6.2473707923 \tag{3.4}$$

$$n^2 C_O R_L LC = 0.2846969462 \tag{3.5}$$

$$n^2 C_O R_L RC + n^2 LC = -21.1211483312 \tag{3.6}$$

$$n^2 C_O R_L + n^2 RC + R_L C = -188.7660261691 \tag{3.7}$$

$$n^2 = 26958.4571934989 \tag{3.8}$$

Their solutions result in values for equivalent components that reproduce the experimental behavior but are not the actual characteristic equivalent parameters, since the curve-fitting is an approximation based on a math model of the PT's behavior within the linear range. The equivalent values are shown in Table 4.

Table 4: PT Equivalent Component Curve-Fitting Results

Component	Final Values
R (Ω)	4.4901334668E-3
L (H)	-2.6603371349E-4
C_O (F)	-6.3540966268E-3
C (F)	2.2750052473
n	164.1903078549

Each of the three sets satisfies the approximate model of the experimental curve and therefore each could be considered appropriate for simulation purposes. The first trial

illustrates just how much the actual response, under unique conditions, differs from the manufacturer's. The tuning parameters might be thought of as adjusting for the changes in the equivalent component values that occur due to the approximate open-circuit operation. The second trial offers a more intuitive approach to evaluating the equivalent component values by extracting information from the frequency response of the PT. It creates a response closer to the actual. The third trial relies on curve-fitting techniques for an approximation to the actual response, from which all the equivalent component values are calculated.

3.3 Dynamic Operation

In the second section, the PT's behavior is simulated under dynamic conditions. By varying n, the deviations between the physical system behavior and model performance are observable and should illustrate where the model fails or succeeds to synthesize an accurate response of the piezoelectric transformer under dynamic conditions. The harsh extremes of space will subject the PT to a wide variation of temperatures. To model this, the n parameter is adjusted and the corresponding frequency response and input impedance is generated. This parameter, shown in the PT as the turns ratio of the coupling transformer in the equivalent circuit, is representative of the electrical-mechanical and mechanical-electrical energy conversion occurring within the PT. It is a product of material properties, device geometry, and temperature. Therefore it is the material properties, device's dimensions, and construction that affect the PT's gain.

Because the research is concerned with temperature's effect on gain, an effort is made to see exactly how temperature affects the device behavior. Chapter two established that the stiffening of the piezoelectric domains causes a decrease in compliance and therefore a rise in resonant frequency and drop in gain magnitude. Attempts to observe temperature's effect on dimension were inconclusive. Therefore, varying n is acceptable for some temperature-related simulations.

Different responses for n are simulated from 45 kHz to 60 kHz and the results for gain and input impedance are shown in Figure 27 and Figure 28, respectively.

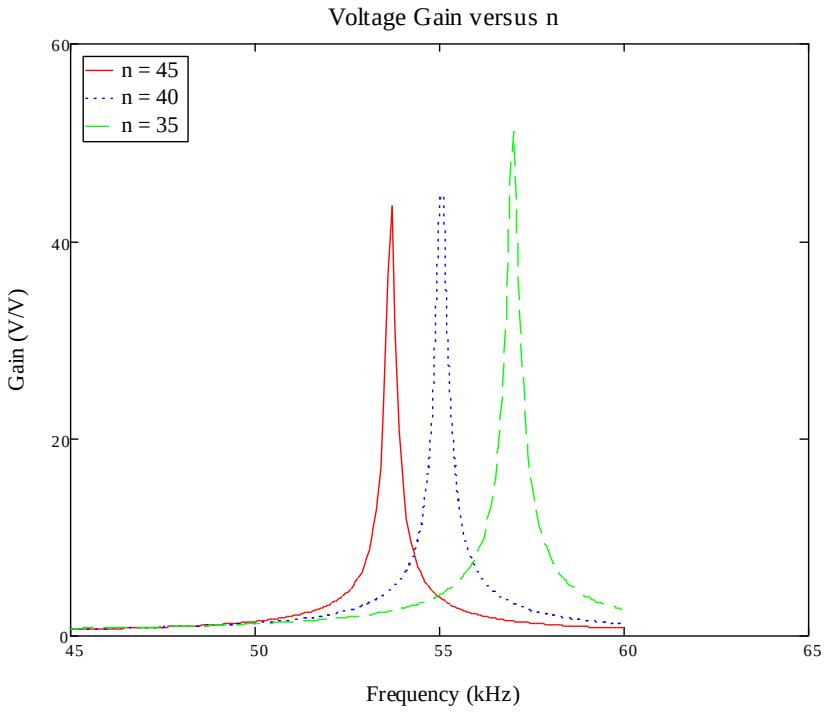

Figure 27: PT Gain as a Function of n

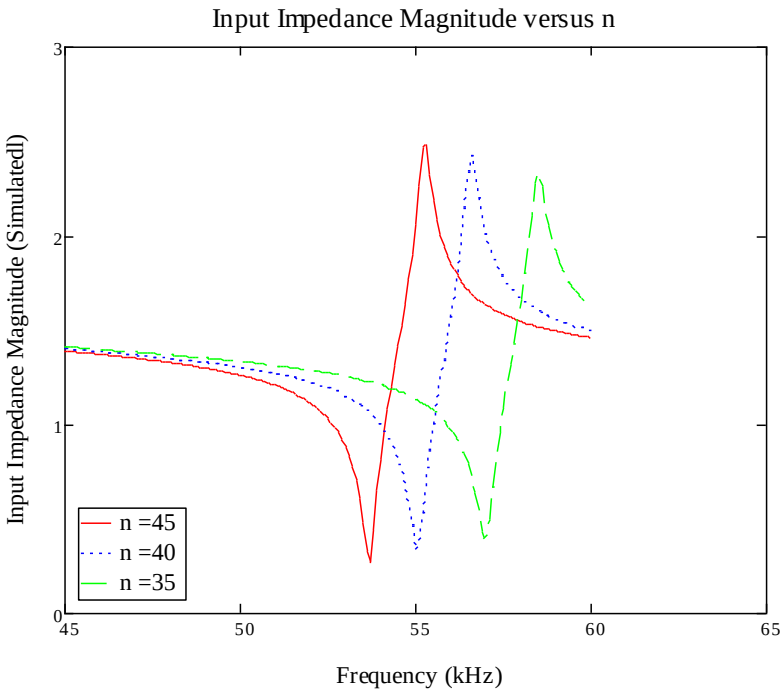

Figure 28: Input Impedance Magnitude as a Function of n

In the resultant simulation, as n decreases, the gain and resonant frequency increases. Because a lowered n is a result of chilling the device, an effect that causes the gain to decrease and resonant frequency to increase in the physical device, the model's response should respond similarly as well. However, as shown in Figure 27, the simulated response does not. Figure 28 shows the effects of decreasing n on the input impedance. Despite having not been able to acquire measurements of the input impedance at cryogenic temperatures, results in other measurements imply what those measurements would reveal an. First, the increase in resonant frequency shown in the frequency response should be exactly the same in the impedance: as the temperature drops, the resonant frequency increases. Second, in chapter two, the fact was pointed out that as the device chills, piezoelectric domains become less mobile and this decreases internal losses. Therefore, as the device cools, the minimum resistance should drop while

the resonant frequency shifts higher. What the simulation shows instead is that with decreasing n, the resonant frequency shifts higher (as expected) and the resonant impedance increases. The frequency of phase shift moves higher as well.

The dynamic results behavior diverges from the expected results for cryogenic temperatures of the PT. Experimental testing would seem to be the only way to determine the actual response in either the frequency response or input impedance.

Based on the results from simulation of the PT's static and dynamic behavior, it is obvious where the model is applicable under certain conditions. In the static case, a limited range of operation where the device is restricted to a particular operation condition, the equivalent circuit is sufficient in reproducing the device's response. Tuning is necessary because even when determining the equivalent component values, the device's behavior is sensitive to operating conditions. For this reason, the manufacturer's values would not suffice and by using a curve-fitting approach, new parameters were found that helped the model better fit the experimental results. The tuning did also provide insight in the parameters that applied to the PT, particularly the extraction of resonant impedance and frequency (in the form of the LC product). In all three situations, the transfer functions were mathematically manipulated to fit the response. Results for simulating thermal effects on the PT show the need for a higher fidelity model that responds with more accuracy to accommodate the rigorous conditions of outer space.

CHAPTER IV

DRIVER CIRCUIT DESIGN

4.1 Theory of Operation and Design

The driver circuit utilizing the piezoelectric transformer consists of two parts, an input signal source driving the PT into mechanical vibration and an output section converting the transformers' output AC into a DC signal usable by the ferroelectric phase shifter.

In the input section there is a need for a high output current, high bandwidth, and high slew rate buffer between the waveform generator and the PT. A benchtop waveform generator (Agilent 33120A) provided the driving signal because the high quality sine wave produced is best for efficiently and effectively driving the PT. A benchtop waveform generator's output frequency and magnitude can be precisely controlled which is convenient for characterizing the device. In addition, no time was needed designing a quality signal source just for a proof-of-concept circuit. However, the waveform

generator alone will not suffice and it is necessary to buffer its signal to the PT. Integrating the buffer along with the rest of the driver circuitry is simple since it lies in the signal path between the waveform generator and PT. In addition, adding the buffer allows for future environmental testing of the components and is one-step closer to actual implementation.

Texas Instruments' OPA547T Operational Amplifier is an excellent choice for the buffer amplifier because of its large gain-bandwidth product (GBP), high slew rate, and large maximum output current. The GBP is 1 MHz, making it more than large enough to span the entire bandwidth of the PTs natural resonant frequency. The Op Amp's slew rate is 6 V/µSec so it can drive the PT over its full dynamic range in under 10 µSec. Slewing in amplifier's output is very undesirable because of the harmonics it would introduce into the PT. The driving signal amplitude need not be any greater than 9 Vpp at a peak frequency of 54.7 kHz. With a peak continuous output current of 0.5 mA, the OPA547T can provide constant regulation over the transformers entire dynamic range of operation. Its negligible output offset voltage is desirable because it will not apply any DC polarization to the PT that would otherwise oppose its AC response. Since the power of the phase shifter controller has a 25 W budget, any energy savings is beneficial. Because the reflectarray power consumption is a matter of scale with regard to phase shifter count, the driver circuits are an important place to consider implementing low power functionality. An Op Amp's quiescent current is the current consumed by the device's own operation, separate from the load. This particular one has a quiescent current of only 10 mA per supply rail making it an acceptable choice for an efficient circuit. The OPA547T also has a wide input voltage range that provides the flexibility of an even

wider range of operating voltages on the PT, so long as the dielectric strength of the ceramic is not exceeded. Aside from its performance, there is also extra functionality with the Op Amp that opens the possibility for future designs. An output enable/disable pin and a programmable current limiting pin are included and may be used in some type of device protection function or current feedback control strategy. The buffer circuit is a unity gain amplifier operates in dual supply mode so that all oscillations are referenced to ground (0 V). The current limiting feature is left disabled (by shorting to the negative rail) enabling maximum output current. The enable/disable feature is unused as well and disabled by shorting to the positive rail [23].

The output circuit is a voltage doubler rectifier explained in [26]. Referring to Figure 29, Cree's CSD01060E Schottky diodes were selected for the rectifiers.

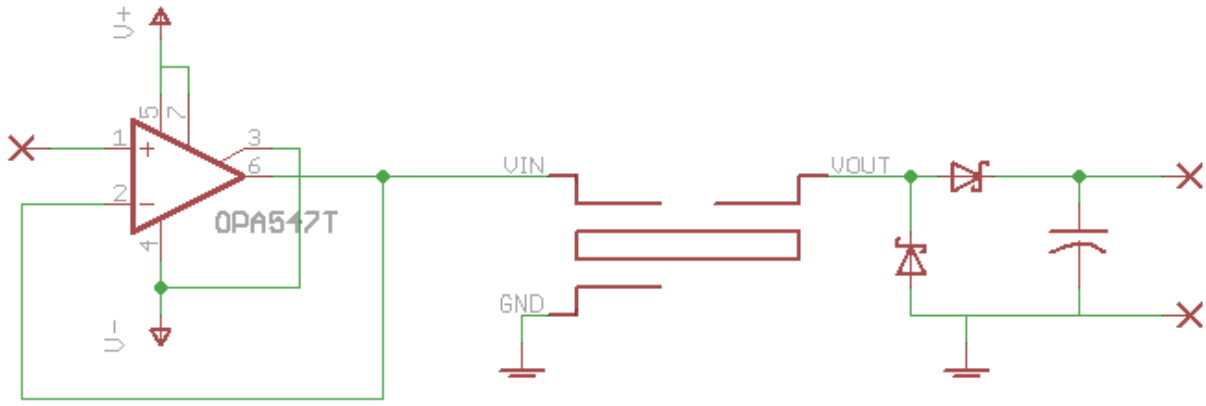

Figure 29: Complete schematic for proof-of-concept driver circuit

Unlike PN junction diodes, Schottky diodes have no depletion region and as a result have no reverse recovery time, negligible off-state capacitance, low forward voltage, and near instantaneous turn off/on recovery times. Typical silicon power diodes

were first used but they failed to switch properly and resulted in a distorted, underperforming output. Because the frequencies of operation are far higher than those intended for normal rectifiers, the zero recovery time ensures that over the entire operational range of the driver circuit, no adverse effects occur in the behavior of the PT and the diodes function properly. Because of the potential for such high voltages on the output, a silicon carbide component is most ideal given its extreme ruggedness. The CSD01060E is a silicon carbide part rated for 600 Volts DC (Vdc), blocking and is used well within its rated operation. The low off-state capacitance is only 80 pF, this means the diode turns on and off quickly and that the equivalent junction capacitance is small enough to effectively block the high frequency signal.

The output capacitor does not have many constraints placed upon it, so long as it is sufficiently large enough to provide effective smoothing on the output (regulation is of little concern as the phase shifter is over very high impedance over its entire range of operating conditions) and is rated for the voltage on the output. The smoothing capacitor is a 500 V, 0.01 μF part. The 500 V rating ensures dielectric breakdown will not occur for the voltage range of operation. The time constant of the output section, the smoothing capacitor and phase shifter (approximated as a 10 MΩ resistor), is much larger than the switching period $1/f$ and therefore, the ripple on the output is negligible.

The whole circuit was laid out using Cadsoft's EAGLE printed circuit board design software and was chemically etched on FR-4 using UV lithography.

4.2 Prototype Performance Evaluation

With the driver circuit complete (shown in Figure 30), the driver's function is evaluated in two schemes of operation.

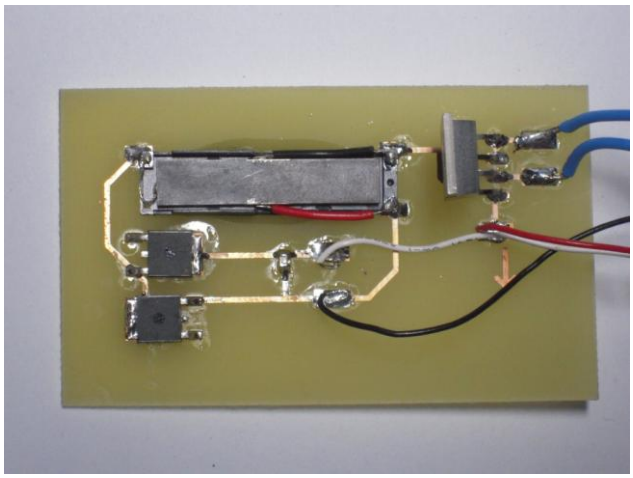

Figure 30: Complete Phase Shifter Driver Circuit

The first is the well familiar fixed frequency, variable input voltage drive signal. The second was fixing the input voltage to the minimum required to reach 300 Vdc at resonance and adjusting the drive frequency to obtain a range of voltages. In the first approach, the input frequency was set to the resonant frequency determined when the PT was out of the cryostat (54 kHz). The results are shown in Figure 31.

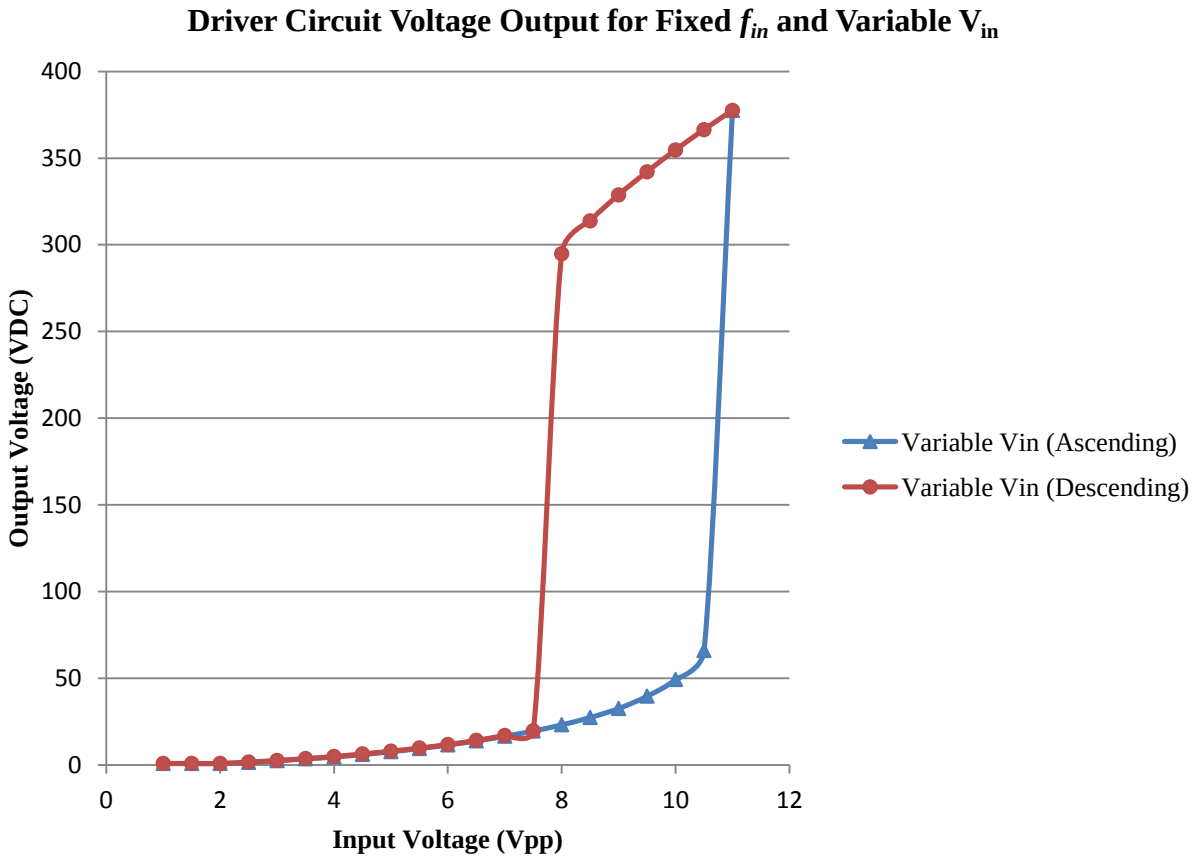

Figure 31: Driver Circuit Voltage Output For Fixed Fin and Variable Vin

From the response it is clear the circuit exhibits hysteresis and that a memory is present in the device. This behavior complicates phase shifter performance.

The second scheme's results are shown in Figure 32 and they show no memory effects.

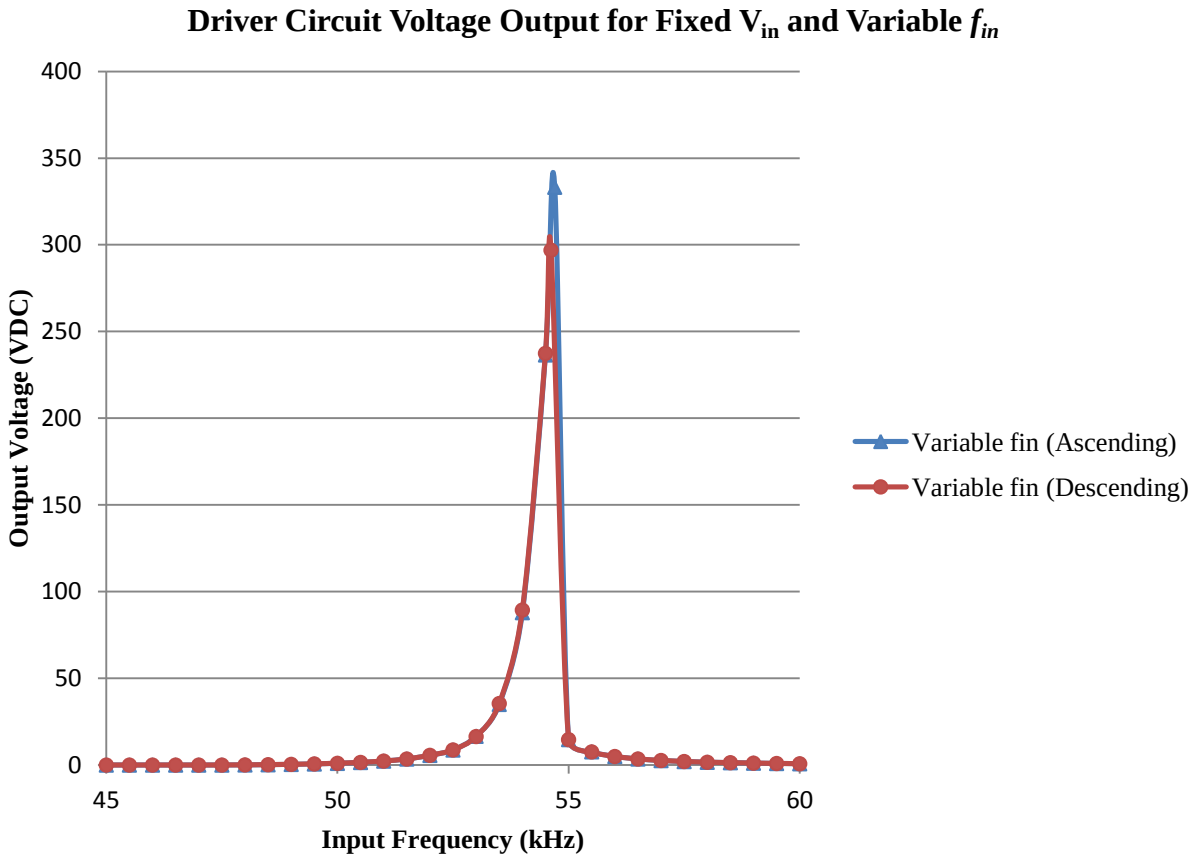

Figure 32: Driver Circuit Voltage Output for Fixed Vin and Variable Fin

So, although both are able to reach the full dynamic range required for the phase shifter's correct operation, the variable frequency scheme proves the more effective due to the absence of hysteresis. From Figure 32, the range of frequencies over which the driver switches in order to sweep the whole range of voltages is narrow, and because there is no hysteresis, the control effort in any future controller setup is simplified.

4.3 Integration with the Ferroelectric Phase Shifter

Now with the driver circuit evaluated, the phase shifter is connected and the whole circuit's performance is determined. Leads, connected to the bias tees, are wired directly to the output of the rectifier. From the driver circuit's point of view, there should be little difference between the high impedance probe and the phase shifter, so the behavior should be the same. The phase shifter was driven using both the fixed frequency and fixed voltage methods. The phase shift is measured at 27.5 GHz using an Agilent E8561A vector network analyzer. The frequency was adjusted so that the output voltage reached the desired level. Starting with Figure 33, a drive frequency of 42.79 kHz, produced 0.1 Vdc on the output and 139.21 degrees on the phase shifter. This is essentially the ground state for the phase shifter and represents a relative phase shift of zero. It includes insertion phase not capable of being de-embedded because of differences between the calibration plane and the measurement plane. At 46.01 kHz the voltage is 1 Vdc and 139.39 degrees phase shift result, shown in Figure 34. Figure 35 is the result of 50.48 kHz, which generates 10 Vdc and results in 144.98 degrees phase shift. Shown in Figure 36, with 52.21 kHz, 50 Vdc is generated and 165.71degrees result. In Figure 37, a drive frequency of 52.82 kHz, produced 100 Vdc on the output and -179.24 degrees on the phase shifter. At 53.46 kHz, the voltage is 300 Vdc and -123.1 degrees phase shift result, shown in Figure 38.

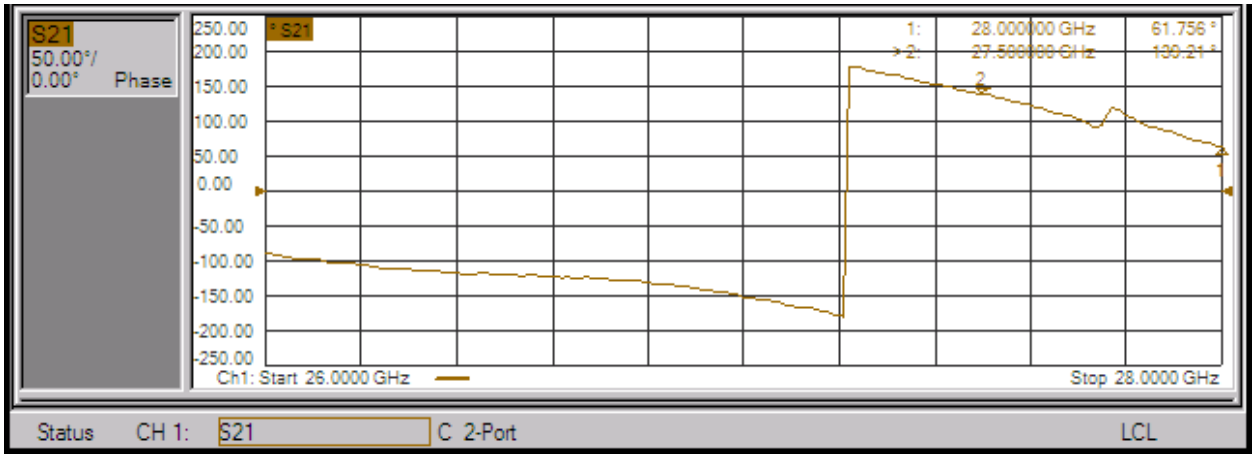

Figure 33: Fin = 42.79 kHz, 0.1 Vdc Applied, 139.21 Degrees Phase Shift Result

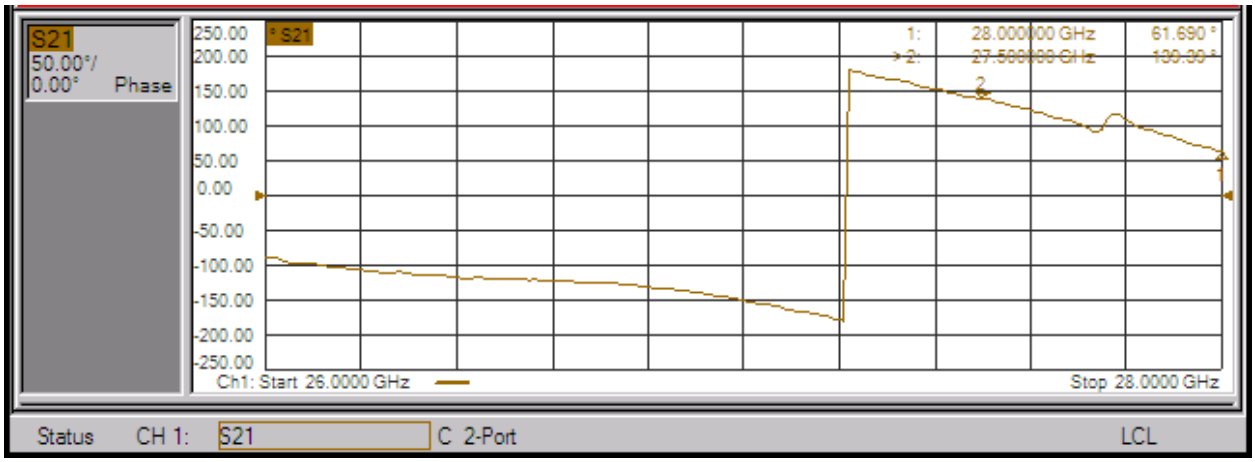

Figure 34: Fin = 46.01 kHz, 1.0 Vdc Applied, 139.39 Degrees Phase Shift Result

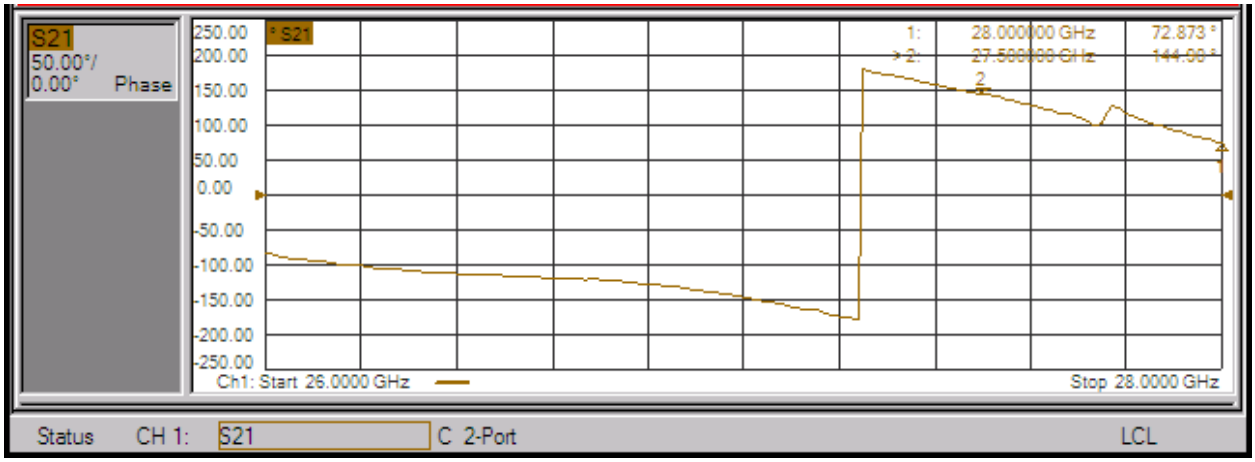

Figure 35: Fin = 50.48 kHz, 10.0 Vdc Applied, 144.98 Degrees Phase Shift Result

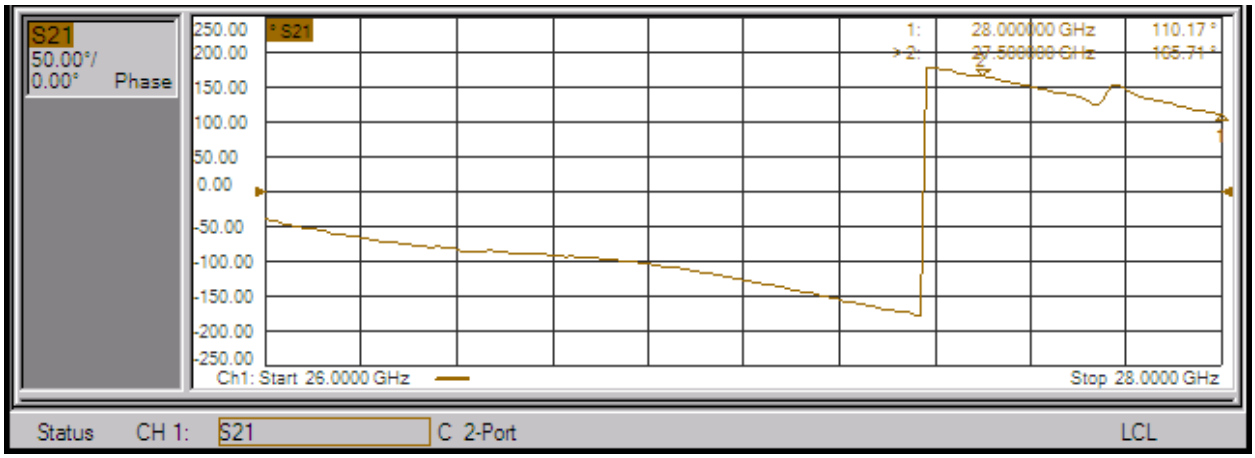

Figure 36: Fin = 52.21 kHz, 50.0 Vdc Applied, 165.71 Degrees Phase Shift Result

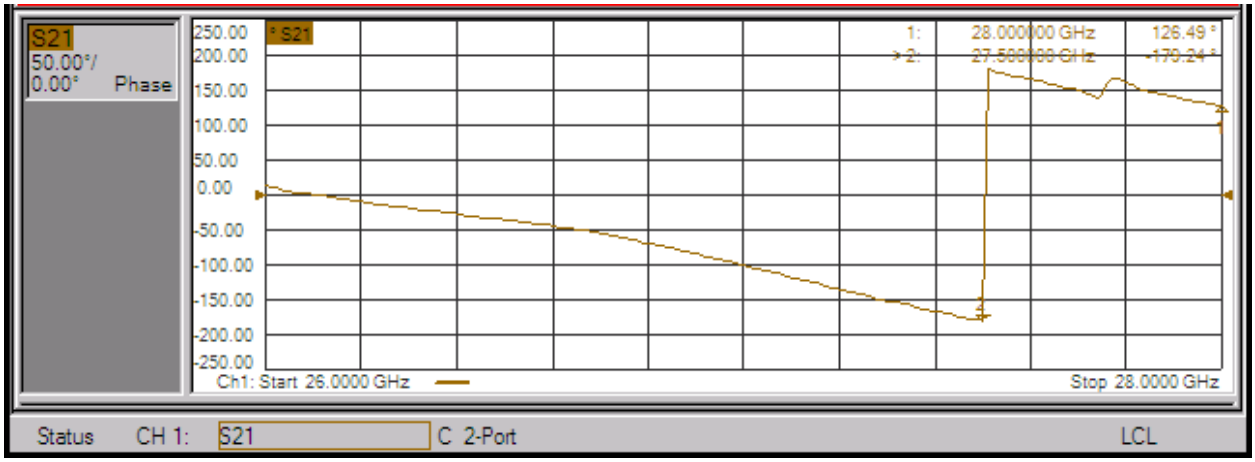

Figure 37: Fin = 52.82 kHz, 100.0 Vdc Applied, -179.24 Degrees Phase Shift Result

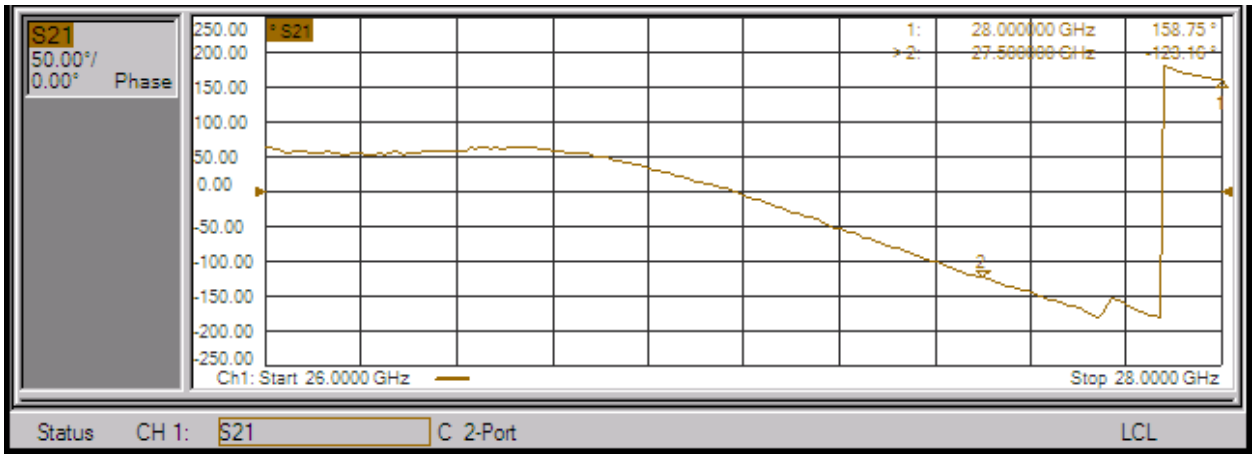

Figure 38: Fin = 53.46 kHz, 300.0 Vdc Applied, -123.10 Degrees Phase Shift Result

Preliminary results were successful with the driver achieving an output voltage from 0 to 300 Vdc and accomplishing about 98 degrees of phase shift (+139 to -123). Results were limited to less than a full 2π, but this is due to the phase shifter's design and not the driver circuit.

CHAPTER V

CONCLUSION

5.1 Summary

This research successfully demonstrates the implementation of a piezoelectric transformer in a ferroelectric phase shifter driver circuit. A proof-of-concept driver circuit, based on the PT, outputs voltages in excess of 400 Vdc from an input ranging from 1 to 10 Vac. This causes the phase shifter to insert up to 180 degrees of phase shift at Ka-band.

Research started with a literature review, where the fundamentals of piezoelectric and ferroelectric materials were investigated. This knowledge compliments further readings about piezoelectric transformers. Important to this work was other research studying the device's behavior and its applications. The next section discusses the need to characterize the piezoelectric transformer over temperature. Because the PT is nonlinear, particularly in response to its temperature, it is necessary to determine the frequency response and input impedance. Experiments were designed to measure the gain versus

frequency at room and cryogenic temperatures and the input impedance versus frequency at room and cryogenic temperatures as well. An attempt was also made at measuring the device's physical response to cryogenic temperature by using a laser radar; without any conclusive results, unfortunately. Chapter two explored the equivalent circuit in greater detail and its applications. The theoretical response from the model is compared to the experimental response. By taking into consideration the nonlinearities that are present in the physical system that are not present in the model, an attempt is made at reconciling the two. This leads to the next step of extracting new equivalent circuit values that will generate the same response for the piezoelectric transformer's particular point of operation in the experimental operation phase. In section three, the design, theory of operation, and evaluation of a proof-of-concept driver circuit for the ferroelectric phase shifter is presented. Based partly on a well-established doubler-rectifier design and using the data gathered in the previous section, a driver circuit was laid out. Test points were included in the design to allow for measurements as well as interfacing with the phase shifter itself. Two modes of operation for the driver circuit were realized: one where the input signal's frequency was kept fixed at resonance and the magnitude varied, and the other where the magnitude was kept fixed and the frequency adjusted. The presence of hysteresis in the driver circuit's output when operating in the fixed frequency mode makes the fixed input voltage mode preferable. Efficiency data in the form of current drawn by the PT's driver circuit was measured as well. In chapter four, the phase shifter was integrated with the driver circuit and functionality is tested by measuring the change in phase shift as the circuit applies different voltages.

This work was presented as an invited talk on August 3, 2011 at the 2011 International Symposium on Integrated Functionalities in Cambridge, England. It will be published in a 2012 edition of *Integrated Ferroelectrics* (Volume 134, Issue 1).

5.2 Future Research and Work

This research, apart from developing a low power, lightweight and high-performance driver circuit using a piezoelectric transformer, furnishes the novel design concept of marrying ferroelectrics and piezoelectrics within a single application, a pairing that can evolve into many more applications. Also novel in this work are the cryogenic characterization of a piezoelectric transformer and the evaluation of multiple modes of operation, namely the fixed frequency-variable voltage and fixed voltage-variable frequency modes. The cryogenic exposure mimicked the effects that the PT would encounter in the cold of space. The two driving modes revealed how the PT functions in operation and how the hysteresis manifests itself in the device. Through this work, a unique and new alternative to magnetic components in ferroelectric phase shifter drivers is offered.

With the completion of the driver circuit, the issue of future work arises. Areas that warrant future pursuits are the characterization of the piezoelectric transformer, further development of the driver circuit, and the implementation of the driver circuit with the ferroelectric reflectarray antenna.

By better characterizing the PT, a greater understanding of its behavior is established. This knowledge could help in the improvement of the driver circuit design. Using precision thermo-mechanical data, a greater insight to the device's frequency response at cryogenic temperatures is established. This information might be useful in creating improved computer models of the device or when selecting piezoelectric transformers for similar applications. However, because the laser radar failed to scan the PT with the precision required for an accurate dimension reading, an alternative might be to use a microscope with an eyepiece micrometer.

Modeling is a powerful tool for engineering analysis and design. As discussed in chapter three, the equivalent circuit model for the PT is limited to a narrow, linear range of operation. Further complicating modeling efforts is the presence of a split-resonance at cryogenic conditions, a non-linear situation. This suggests a model is two, coupled, resonant circuits. It is this coupling that is either dampened or exacerbated by the effects of temperature. Future research of dual resonance in piezoelectric transformers should investigate the following: its cause, whether or not it is common in all types of PTs, and if it can be accurately modeled. Appendix A provides a preliminary attempt at modeling the dual-resonance encountered experimentally. The peculiar impedance of the device provides insight into an improved model. What it suggests is a series resonance followed by a parallel one. Ascertaining the causes of this behavior and how to model it provide invaluable information on the PT's functionalities. By taking advantage of the device's behavior, better driving circuitry (perhaps for improved efficiency or performance) can be developed. An improved model offers the parameters for better controller design. It

also leads to improved output circuitry, making the device available for broader applications or improving its performance.

Now that it has been shown the piezoelectric transformer can bias a ferroelectric phase shifter, further work lies in maturing this technology. One place to start is device control and driving. Chapter two made the point that the device is very nonlinear over temperature and frequency therefore, in order to be sure the phase shifter is outputting the required voltage, regardless of temperature, some type of control scheme is necessary. Whether this controller is integrated with the phase shifter or off board, is left to future design but it will have to compensate for the change in resonant frequency and gain by adjusting the driving frequency and amplitude. This might be accomplished via a feedback loop where the output voltage is compared to a set point and using either temperature measurements, input current readings, or both, the drive signal is adjusted. The rectifier circuitry might also be another place for improvement. The rectifier-doubler was only chosen because it was an established, effective means to supply high voltage DC to a high impedance load. It may be, however, that a better topology could be realized that affects PT behavior in some unforeseen, positive way. The driving signal, currently supplied by the waveform generator and buffered by an Op Amp, might be practically implemented in a number of ways. A signal bus could supply entire groups of drivers and therefore be located away from the PTs. Alternatively; a signal source might be integrated with the PT and have only control signals routed to it. If the driver could eliminate the buffer circuit while providing the source current and signal properties, energy and cost savings could be realized. Future research might also reveal interesting options in the driving signal. Despite current understanding that a single tone is the

preferred way to drive the device, perhaps there may be use in driving the PT with a polytone signal. An example of such a use is a control scheme that derives the PT's operating information by comparing two or more signals injected into the PT. Another use is using a polytone signal as a way to boost the output voltage. Despite being a niche technology, a few companies do offer a selection of piezoelectric transformers with variations based on poling, construction, and piezoelectric properties. Among the PT product lines, there may be a device better suited to this research's purpose than the SMMTF53P2S40. Perhaps there is a PT with higher input impedance and therefore a smaller Q and lesser current draw, or one that is not as affected by temperature.

Once the driver circuit reaches the necessary level of functionality, it can be integrated with the phase shifter. A way must be found to attach the drivers to the backplane of the reflectarray, as this configuration is optimal for performance and packaging reasons. An approach must also be found to address each driver circuit and to maintain the phase shifter's performance. The driver circuit will also have to be evaluated for space and flight worthiness, which may necessitate a redesign that includes the substitution of radiation-hardened components.

By successfully demonstrating how a driver circuit based on piezoelectric transformer technology can bias a ferroelectric phase shifter, the groundwork is laid for a myriad of applications in analog and power electronics.

REFERENCES

1. Robert Romanofsky and A.H. Qureshi, "A Model for Ferroelectric Phase Shifters," *IEEE Transactions On Magnetics*, vol. 36, no. 5, pp. 3491-3494, September 2000.

2. Robert R Romanofsky, "Advances in Scanning Reflectarray Antennas Based on Ferroelectric Thin Film Phase Shifters for Deep Space Communications," NASA, Cleveland, Technical Memorandum 214983, 2007.

3. Bernard Jaffe, "A Primer on Piezoelectricity and Piezoelectric Ceramics," Morgan Electro Ceramics, Technical Publication TP217,. [Online]. www.morgan-electroceramics.com

4. Robert R Romanofsky, "Array Phase Shifters: Theory and Technology," NASA, Cleveland, Technical Memorandum 214906, 2007.

5. Donald Priebe, "Reflectarray Controller Operations & ICD Document," ZIN Technologies, Inc., Brookpark, AST-OPS-103, 2003.

6. Morgan Electro Ceramics, "Piezoelectricity," TP-238,. [Online]. www.morgan-electroceramics.com

7. James R Phillips, "Piezoelectric Technology Primer," CTS Wireless, Albuquerque, NM, May 2000. [Online]. http://www.ctscorp.com/chn/components/pzt/downloads/Piezoelectric_Technology.pdf

8. APC International, Ltd., *Piezoelectric Ceramics: Principles and Applications*.: APC International, Ltd., 2002.

9. Murata Manufacturing Co., "Piezoelectric Ceramics (PIEZOTITE) Sensors," Catalougue No. P19E-9. [Online]. www.murata.com

10. E.L. Horsley, M.P. Foster, and D.A. Stone, "State-of-the-art Piezoelectric Transformer Technology," in *European Conference on Power Electronics and Applications*, Aalborg, DK, 2007, pp. 1-10.

11. Gregory Ivensky, Isaac Zafrany, and Shmuel Ben-Yaakov, "Generic Operational Characteristics of PIezoelectric Transformers," *IEEE Transactions on Power Electronics*, vol. 17, no. 6, pp. 1049-1057, November 2002.

12. I Kartashev, T Vontz, and H Florian, "Regimes of piezoelectric transformer operation," *Measurement Science and Technology*, vol. 17, no. 8, pp. 2150-2158, July 2006.

13. Steiner & Martins Inc. (2011, February) RE: "Thick" PT Input Capacitances. Email.

14. Steiner & Martins, Inc. (2010, October) Multilayer piezoelectric transformer material - 1931. Email.

15. Steiner & Martins, Inc. (2010, October) RE: Multilayer piezoelectric transformer material - 1931. Email.

16. Hyun-Woo Joo, Chang-Hwan Lee, Jong-Seok Rho, and Hyun-Kyo Jung, "Analysis of Temperature Rise for Piezoelectric Transformer Using Finite-Element Method," *IEEE Transactions on Ultrasonics, Ferroelectrics, and Frequency Control*, vol. 53, no. 8, pp. 1449-1457, August 2006.

17. Morgan Electro Ceramics, "Piezoelectric and dielectric properties of Lead Titanate Zirconate at low temperatures," Technical Publication TP-224,. [Online]. www.morgan-electroceramics.com

18. Matthew W Hooker, "Properties of PZT-Based piezoelectric Ceramics between -150 and 250 C," Lockheed Martin Engineering & Sciences Co., Hampton, VA, NASA Contractor Report 208708, 1998.

19. Kuo-Tsai Chang, "Effects of Load Resistance on Step-Up Voltage Gains of Rosen-Type Piezoelectric Transformer," in *IEEE International Conference on Industrial Technology*, Hong Kong, Hong Kong, 2005, pp. 1080 - 1085.

20. E.L. Horsley, M.P. Foster, and D.A. Stone, "A frequency-response-based characterisation methodology for piezoelectric transformers," in *2nd Electronics System-Integration Technology Conference*, Greenwich, UK, 2008, pp. 959-962.

21. Morgan Electro Ceramics Inc. (2007, November) Morgan Electro Ceramics Inc. [Online]. http://www.morganelectroceramics.com/resources/literature/

22. Steiner & Martins Inc. (2010, October) Multilayer piezoelectric transformer material - 1931. Email.

23. Texas Instruments Inc. (2005, July) Texas Instruments Inc. [Online]. http://www.ti.com/product/opa547

24. D.A. Berlincourt, "General Description of Piezoelectric Transformers," Morgan Electro Ceramics , Technical Publication TP-244, 1999.

25. I Kartashev and T Vontz, "Regimes of piezoelectric transformer operation II," *Measurement Science and Technology*, vol. 20, no. 5, pp. 1-14, April 2009.

26. Gregory Ivensky, Moshe Shvartsas, and Shmuel Ben-Yaakov, "Analysis and Modeling of a Voltage Doubler Rectifier Fed by a Piezoelectric Transformer," *IEEE Transactions on Power Electronics*, vol. 19, no. 2, pp. 542-549, March 2004.

27. Jesús Manuel González-Miranda, *Synchronization And Control Of Chaos: An Introduction For Scientists And Engineers*.: Imperial College Press, 2004.

APPENDIX

The appendix addresses continued work in developing a model of the double resonant behavior of the piezoelectric transformer. Although beyond the scope of this work, the PT's double resonance bears mentioning because of the strong semblance that the results in [27] have to those in chapter two and the profound effect this effect could have on device operation that might limit its applications to space technology. So with further effort, it may be possible to build off of the aforementioned work and use it in investigating a potential model for the double resonant behavior for the purposes of understanding the device better, aiding in the development of electronics, and controlling the device.

The double resonance began appearing in the extreme cryogenic temperatures used in chapter two. It was postulated that the extreme cold affected the mechanical coupling between each half of the device, causing them to resonate independently of each other rather than as one whole piece. In [27], the author devotes a chapter to analyzing coupled and driven harmonic oscillators by using two coupled mass-spring-damper mechanical systems as a model (Figure 39).

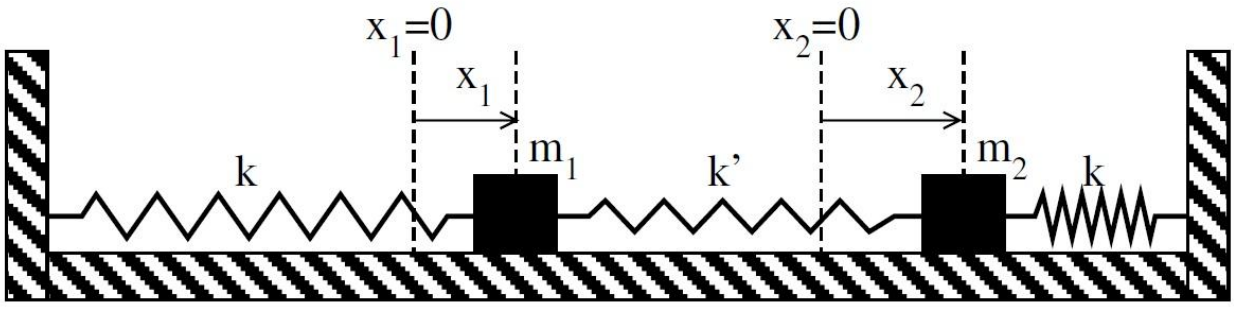

Figure 39: Coupled Mass-Spring-Damper System

Analyzing the author's model yields the equations of motion for the above system and they are given in (A.1) and (A.2).

$$F_1 - kx_1 - k'(x_1 - x_2) - B_1 \frac{dx_1}{dt} - m_1 \frac{dx_1^2}{dt^2} = 0 \quad \text{(A.1)}$$

$$k'(x_1 - x_2) - kx_2 - B_2 \frac{dx_2}{dt} - m_2 \frac{dx_2^2}{dt^2} = 0 \quad \text{(A.2)}$$

Here F_1 is the applied force to block m_1, and B_1 and B_2 are the friction coefficients for blocks one and two, respectively. The author manipulates the equations to their form in (A.3) and (A.4) and provides a general solution in equations (A.5) and (A.6), respectively.

$$\frac{d^2x_1}{dt^2} + \boldsymbol{\omega_0^2 x_1} + \boldsymbol{\kappa^2(x_1 - x_2)} = \mathbf{0} \quad \text{(A.3)}$$

$$\frac{d^2x_2}{dt^2} + \boldsymbol{\omega_0^2 x_2} + \boldsymbol{\kappa^2(x_2 - x_1)} = \mathbf{0} \quad \text{(A.4)}$$

$$x_1(t) = A_1 \sin(\omega_1 t + \delta_1) + A_2 \sin(\omega_2 t + \delta_2) \quad \text{(A.5)}$$

$$x_2(t) = -A_1 \sin(\omega_1 t + \delta_1) + A_2 \sin(\omega_2 t + \delta_2) \quad \text{(A.6)}$$

For an initial application, the above model is manipulated to match the frequency response for the piezoelectric transformer. To do so, the experimental values for each resonant peak in the experimental response (Figure 1) are substituted in Equation (A.6) and evaluated using Mathcad. A_1 and A_2 are the peak amplitudes and are set equal to one; δ_1 and δ_2 are the relative phase shifts and are set equal to zero. For the resonant frequencies, ω_2 is related to ω_1 by the equation $f_2 = \sqrt{f_1^2 + 2\kappa^2}$, where κ is the coupling coefficient [27]. By assigning the first of the split resonance values to f_1(54.9 kHz), κ can

then be varied (8650) until f_2 matches the experimental value (56.3 kHz). The time domain response is shown in Figure 40 and the frequency response is shown in Figure 41. All results are computed using Mathcad.

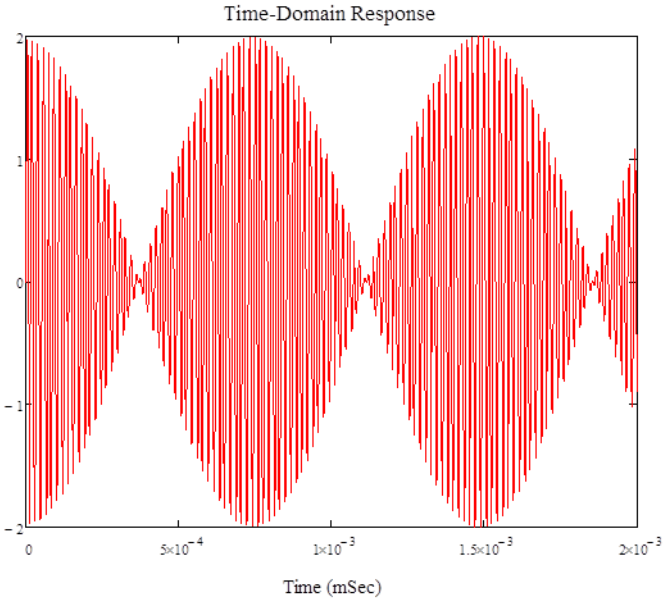

Figure 40: PT Dual-Resonance Time Domain Response

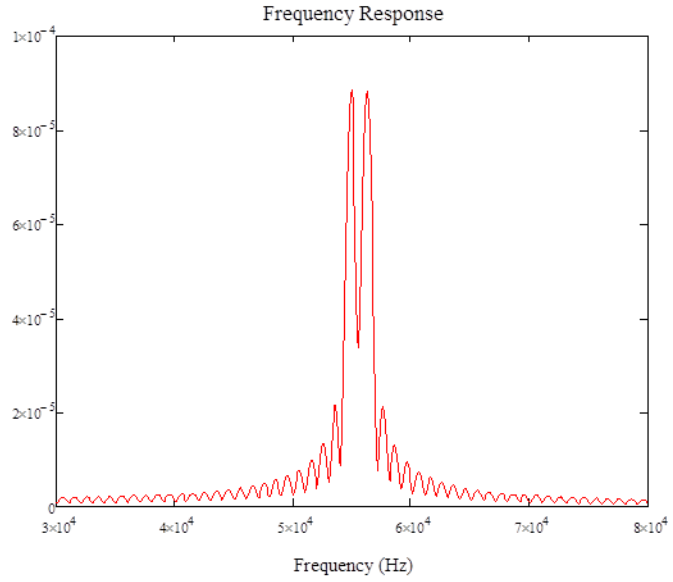

Figure 41: PT Dual-Resonance Frequency Domain Response

What results are very clearly the split resonant peaks of the cryogenically operating piezoelectric transformer. This shape can be compared with the experimental response of Figure 17.

Based off of these results, future work could investigate relating the equations' parameters to those of the actual piezoelectric transformer, further investigating the theory of the device's operation and developing an improved model of the coupling and performance of the PT at cryogenic temperatures.

The author's work [27] can be extended into the electrical domain, yielding a circuit that is familiar from earlier sections of this work. An equivalent analog of the mechanical systems can be written by replacing linear displacement (x) with charge (q), allowing an equivalent electrical circuit to model the same system. From equations (A.1) and (A.2), the equivalent electrical equations are given below.

$$V - \frac{1}{C_1}q_1 - R_1\frac{dq_1}{dt} - L_1\frac{d^2q_1}{dt^2} - \frac{1}{C_2}(q_1 - q_2) = 0 \tag{A.7}$$

$$\frac{1}{C_2}(q_1 - q_2) - \frac{1}{C_3}q_2 - R_2\frac{dq_1}{dt} - L_2\frac{d^2q_2}{dt^2} = 0 \tag{A.8}$$

What results are a set of loop equations that describe the equivalent circuit shown in Figure 42.

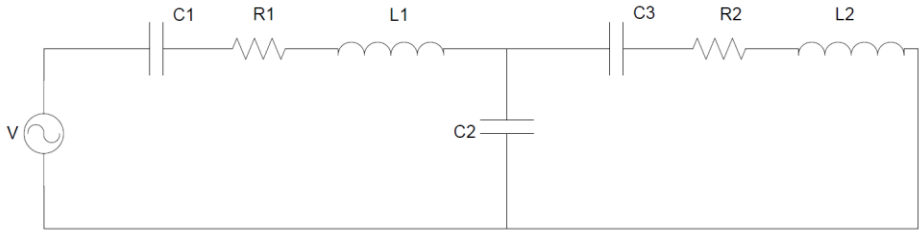

Figure 42: Equivalent Electrical Circuit

This is not unlike the coupled piezoelectrics present in the PT and therefore may make a good template for the cryogenic model of the device.

Such a circuit might aid future work in the design of future electronics based on the PT operating at cryogenic temperatures